Departamento de
Informática e Ingeniería
de Sistemas
Universidad Zaragoza

Escuela de
Ingeniería y Arquitectura
Universidad Zaragoza

Tesis de Fin de Máster
Máster en Ingeniería de Sistemas e Informática
Curso 2010/2011

Construcción de Mapas de Cobertura para Comunicaciones Inalámbricas

Coverage Map Building for Wireless Communications

Carlos Ernesto Rizzo Bobbio

Director: Dr. José Luis Villarroel Salcedo

Departamento de Informática e Ingeniería de Sistemas
Escuela de Ingeniería y Arquitectura
Universidad de Zaragoza

Noviembre de 2011

Construcción de Mapas de Cobertura para Comunicaciones Inalámbricas

RESUMEN

Conocer ciertas características sobre cómo es la propagación de la señal en determinados entornos es de vital importancia para el uso efectivo de una red de comunicaciones inalámbrica. Dependiendo de la complejidad del medio podemos utilizar como guía uno o varios modelos de propagación, pudiéndose llegar a buenas aproximaciones sobre el comportamiento de la señal. Bien sea para desarrollar modelos (empíricos o deterministas) o validarlos, se requieren mediciones experimentales. En otros casos no se dispone de un modelo de propagación, por lo que la única opción radica en tomar mediciones prácticas. Cualquiera sea el caso, a través de la representación de estas mediciones en función de la posición obtenemos lo que se suele llamar un mapa de comunicaciones o mapa de cobertura.

Situados en este contexto, en este trabajo se desarrollaron herramientas para la construcción de mapas de comunicaciones a gran escala y a pequeña escala. Pensando en una solución modular, se desarrollaron diversos módulos para el meta sistema operativo ROS y se implementaron en un vehículo real todoterreno, y en un robot Pioneer P3AT.

Se realizaron pruebas en un ambiente de especial interés para el grupo RoPeRT (Robotics, Perception and Real Time) de la Universidad de Zaragoza: el túnel ferroviario de Somport, que conecta Francia con España. Se obtuvo un mapa de cobertura a gran escala de una sección de especial interés, de unos 2.5 km de largo con cambio de pendiente, y uno más detallado a menor escala de una sección de 1 Km, donde aparecen atenuaciones importantes.

Se compararon los resultados con un modelo de propagación basado en “Ray Tracing” (trazado de rayos), desarrollado por Valenzuela (1993). Se obtuvieron similitudes como la existencia de un notable fading, pero a la vez diferencias que dan importancia a las mediciones realizadas, como la ubicación de este fading y diversas atenuaciones que no aparecen en las simulaciones. Se verificó la repetibilidad de estos fenómenos realizando diversos experimentos, inclusive en días diferentes, cuestión que no se ha sido tratada con importante énfasis en la literatura.

También se encontró que, debido a variaciones transversales, aplicando una diversidad espacial muy superior a la de las tarjetas comerciales, podemos mejorar la calidad de señal en la mayoría del trayecto estudiado.

Los resultados obtenidos pueden ser utilizados tanto para el despliegue óptimo de redes inalámbricas, hasta inclusive para el desarrollo de técnicas de navegación para equipos multi-robot manteniendo la comunicación.

Coverage Map Building for Wireless Communications

ABSTRACT

Knowing certain characteristics about signal propagation in specific environments is crucial in order to make effective utilization of a wireless network. In some cases, one or several propagation models may be used, which can provide good approximations to signal behavior. To develop these models (either empirically or in a deterministic way) and evaluate its reliability, experimental measurements are required. In other cases, due to environment complexity, a specific model isn't available and practical measurements must be done. In any case, representing these measurements as a function of position, we obtain what is usually called a communication map or coverage map.

In this context, this work aims the development of tools for building communication maps. Based on a modular solution, various modules were developed for meta-operating system ROS, and were implemented over a real all-terrain vehicle, and a Pioneer P3AT robot.

Tests were made on a special scenario of interest for University of Zaragoza research group RoPeRT (Robotics, Perception and Real Time): the Somport railway tunnel, which connects Spain with France. At first, a large scale coverage map of a zone of interest was obtained (about 2.5 Km long with a change in slope). Then, a smaller and more detailed map within this zone was built, where important fadings and phenomena appeared.

Results were compared to a straight tunnel Ray Tracing model developed by Valenzuela (1993). We found important similarities, like the existence of a notable fading, but at the same time important differences, such as the exact location of this fading and other fadings that don't appear in simulations. Repeatability of these phenomena was proved by performing different experiments, even on different days. This has not been significantly addressed in the revised literature.

We also found that because of transversal variations, applying large scale diversity for antennas, good quality signal can be achieved in almost the entire studied area.

Results obtained in this work can be use from optimal deployment of a wireless network, up to the development of multi-robot navigation strategies under communication constrains.

AGRADECIMIENTOS

Primeramente a mis padres, Tony y Chelo, a mis hermanos, Gabriel y Carolina; y a Eugenia Valentina, por el apoyo emocional y familiar muy necesitado, en visitas y por Skype, brindado a lo largo de todo el proyecto.

En especial, a los profesores Carlos Sagues y José Luis Villarroel. Gracias a ustedes me encuentro en estos momentos aquí, y sin su tutoría el proyecto no se hubiese podido llevar a cabo.

Al grupo RoPeRT, por brindarme la oportunidad de desarrollar este proyecto y cuyos comentarios y sugerencias fueron vitales para la realización exitosa del mismo.

A José Luis, Danilo, Domenico y Luis, por toda la ayuda brindada en el famoso Túnel y aguantar horas de frío, oscuridad y polvo para ayudarme a probar las herramientas.

A Daniel Cestari y Antonio Baez, por su ayuda técnica en ciertas partes.

Finalmente, pero no menos importante, a mis compañeros especiales de siempre: Den, Mily, Ceci, Vane, Tony, Diego, Juan, Elías, Daniel, Alejandro “El Micri”, El Gordo Dassy; a los que no he visto mucho pero han servido de gran apoyo… Mariale; y a los nuevos: Roberto, Rosita, Boris, Danilo, Dome, Pablo, Luis, Mayte, El César, Henry, El otro Luis, Agus… Ha sido un placer conocerlos y gracias a ustedes este año ha sido genial.

Financiamiento

El trabajo aquí presentado es financiado y se desenvuelve en el marco del proyecto “SISTEMAS MULTI-ROBOT EN APLICACIONES DE SERVICIO Y SEGURIDAD - TESSEO” (ref. DPI2009-08126), dentro del subprograma FPI-MICINN, referencia de la ayuda BES-2010-038377.

Funding

The work presented has been supported by the FPI-MICINN Project “TEams of robots for Service and Security missiOns - TESSEO” (ref. DPI2009-08126) under research grant BES-2010-038377.

Contents

List of Figures

Chapter 1

Introduction

Communication networks are crucial for the proper performance of many systems, where an opportune and adequate information exchange is always needed. In many situations, a wired architecture is not feasible, either because is not possible or convenient. This is the case for multi-robot cooperative teams, VANETs (Vehicular Ad-Hoc Networks), communication systems in hostile environment, among others. In these cases, a wireless solution is needed, and this type of networks has become popular in the last years because of its versatility and ease of implementation and deployment.

Among these technologies, WiFi, which operates under the 802.11 standards suite, has become one of the most popular. One reason is because it works on the ISM band (Industrial, Scientific and Medical), which requires no license. Besides, equipment needed to deploy this type of networks has become less expensive because of its massive utilization and commercialization. This has made WiFi preferable over other standards, such as WiMAX, despite they have different characteristics (El-Sayed et al. 2008).

To make optimal utilization of these wireless networks it's desirable to have knowledge of both the nature of the signal as well as the environment where it is spreading. A practical manner to do this is creating coverage maps or communication maps, where signal power as a function of position is represented for a specific environment.

Several studies have been made about signal propagation. Antenna polarization, operation frequency, material characteristics and geometry of the environment have all been taken into account. Nevertheless, there are few papers that describe the tools used to derive these studies, and according to our literature revision, there is no such tool designed to facilitate the construction of these maps, and do so autonomously. In human-made case, it's a consuming and prone error job. This is the reason why in most of the cases a sensor network is deployed, or a robot is used but with previous knowledge of the place (Holland et al. 2006; Lun-Wu Yeh et al. 2009).

These type of solutions are not suitable for some environments. For instance, if the coverage area is too large, it may result economically unfeasible to deploy a sensor network. Because of hostile conditions human presence may be compromised, so it is better to be

performed in an autonomously or semi- autonomously manner. Also, previous map of the site is not always available, so if you add the ability to Simultaneous Localization and Mapping (SLAM), the solution would be much more complete.

In such a context, the aim of this work is to develop a tool that fulfills the above requirements for building coverage maps, and test it on a real scenario. To do this, we explored ways to acquire and analyze characteristics of the wireless signal, as well as a study of propagation phenomena with emphasis in a specific environment: tunnels.

After testing the tools, a large scale coverage map of a special zone in the Somport railway tunnel was obtained (about 2.5 Km long with a change in slope). Then, a smaller and more detailed map within this zone was built, where important fadings and phenomena appeared.

Results were compared to an implementation of a straight tunnel Ray Tracing model, developed by Valenzuela (1993). Important similarities appeared, like the existence of a notable fading, but at the same time important differences, such as the exact location of this fading and other fadings that don't appear in simulations. Repeatability of these phenomena was proved by performing different experiments, even on different days. This has not been significantly addressed in the revised literature.

We also found that because of transversal variations, applying large scale diversity for antennas, good quality signal can be achieved in almost the entire studied area.

The utilization of these tools could influence areas such as the study of phenomena as consistency and repeatability of the signal in certain environments, propagation models development, efficient and optimal network deployment, communication studies in VANETs, optimization and upgrade of coverage maps, localization with communication metrics, and even suggesting navigation techniques in multi-robot teams under connectivity constrains.

This work is structured as follows. In the next section, a state of the art revision is presented, as well as the theoretical bases about signal propagation with the aim of coverage map building. In section 3, the test scenario is described, along with a tunnel propagation model. Later, in section 4, we present the tools developed in order to build communication maps (at a large scale and a small scale). In section 5, results obtained after testing both tools in the Somport tunnel are presented, followed by an analysis of the phenomena observed. Finally, we present our conclusions and future work.

Chapter 2

Related Work

In order to develop the tools mentioned above, a state of the art review was made, as well as a study about link quality metrics and propagation phenomena in different environments.

One of the areas where these type of instruments are widely used is WiFi based localization systems (Howard et al. 2003; Lun-Wu et al. 2009; Matellán et al. 2006; Ocana et al. 2005; Oka and Lampe 2010; Xinrong 2006). In these works, nodes are placed in a specific area emitting frames in broadcast, and measurements are made to determine signal characteristics in some specific positions. Later on, through various approaches (deterministic or probabilistic), the goal is to locate an objective (robot, person, etc.) based on these characteristics (Howard et al 2003).

The first phase in these works is the coverage map creation. Motivation for Ocana et al. (2005) to do so with measurements is the inconsistency between these and a specific propagation model. When the map is built with the aid of robots, teleoperation for navigation is used. In other works the process has been slightly automated, but with the aid of previous information about the area. Lun-Wu et al. (2009) placed some RFID cards on the ground and the robot navigates locating itself with these.

In any case, quality metrics must be known in order to determine wireless signal characteristics, as well as propagation models revision in order to have some idea about propagation in the environment and phenomena that could appear.

2.1 Link Quality Metrics

To represent the quality of the wireless signal there are various metrics, among which are the RSSI (Received Signal Strength Indicator), SNR (Signal to Noise Ratio), PDR (Packet Delivery Rate), BER (Bit Error Rate). There is currently an open debate on which one to use and why (Vlavianos et al. 2008; Wu et al. 2008; Rong-Hou 2008; Borenovic and Neskovic 2009; Liu et al. 2009). The study of these metrics can derive aspects like intelligent routing, rate

adaptation, topology control, load balancing, frequency selection among others (Wapf and Souryal 2009; Vlavianos et al. 2008).

The RSSI is a received power indicator. It is expressed on a numerical scale, which depends on the manufacturer of the network card (Wu et al. 2008). As the RSSI is measured only during packet preamble reception (which is transmitted at a fixed rate of 6 Mbps), it wouldn't be a good indicator when packets are transmitted at much higher rates (Vlavianos et al. 2008).

The SNR is an indicator of the ratio between signal power and noise power. In certain network cards, as the case of Atheros, this indicator is usually highly correlated with the RSSI (Wu et al. 2008).

On the other hand, PDR is an indicator of the received packets over the transmitted packets. Although is not a signal strength indicator, it is easy to implement and gives an idea about link reliability. Besides, it's correlated to other link quality indicators. For instance, Vlavianos et al. (2008) determined that at a transmission rate of 6 Mbps, if the RSSI overcomes certain threshold, PDR is about 100%. This correlation is lost at higher transmission rates due noise susceptibility. In the same way, it has been determined that at certain PDR values, SNR measurements are unreliable (Dhananjay et al. 2003).

Concerning the BER, it expresses the number of erroneous bits over the number of total bits received. However, is difficult to measure it because is not reported by network cards, therefore it requires packet headers changes, drivers modifications, among others (Vlavianos et al. 2008).

2.2 Propagation models

Once link quality metrics are known, it is desirable to have an idea about signal propagation in the environment. To this end, propagation models (either deterministic or empirical) or practical measurements are used.

Deterministic models are those developed through physics laws, studying interactions and propagation of the wave (for example, through Maxwell's equations). These models are the most accurate, but require analysis and study of a large amount of information, both details of the nature of the wave (polarization, amplitude, phase) as well as the environment where it is spreading (geometry, materials). For this reason empirical models are developed, which despite being less accurate, often provide good approximations processing much less information (Rappaport, 2002, chapter 3).

A classification of areas considered for the utilization and development of these models is usually outdoor scenes, indoor, urban and sub-urban (Hidayab et al. 2009; El-Sayed et al. 2008).

Outdoor scenarios are usually the simplest to analyze, and one of the most used models is the Free Propagation Model. This model yields good results when specific conditions

are met, such as a 60% clearance of the first Fresnel zone, obstacle avoidance, etc., but because of this is inaccurate for indoor cases (Karia et al. 2010).

For indoor scenarios, the Log-distance Path Loss Model is widely used with good results. In this model, the power decays logarithmically with distance, at a rate determined by a Path Loss Coefficient (experimentally determined and usually tabulated for most common scenarios). For urban and sub-urban areas, Okumura-Hata model yields good approximations (El-Sayed et al. 2008).

In some cases (usually indoor), propagation models are valid but not in all areas. For instance, Zvanovec et al. (2003) determined the Path Loss Coefficient for an office building. Predictions using the Path Loss Model were correct in all areas except for one, the corridor, where in the reality attenuation was much less than the modeled. This is because there are some scenarios that, due to its geometry and characteristics, act as a waveguide (Zhang et al. 1998). This is the case for tunnels, which result of special interest for our research group.

Several studies have been made about tunnels, both in a practical and theoretical way. Geometry and symmetry of the area, material conductivity and permittivity constants, as well as wave characteristics result of special interest.

One type of tunnel propagation study is based on modal theory, but it's too complicated to develop. A simpler model based on Ray Tracing, developed by Valenzuela (1993), has been successfully and widely used. It's based on geometric optics, and considers tunnel walls as reflective surfaces. The total power received is calculated as the result of the sum of the direct and reflected rays. Depending on the complexity of the environment, ray-launching or ray-imaging tracing algorithms are used to calculate these rays (Kermani and Kamarei 2000). Nevertheless, when there is no Line of Sight (LOS) between transmitter and receiver these calculations can become complicated, because when the wave propagates the main mechanisms it suffers from are reflections, diffractions and scatterings (Rappaport, 2002, chapter 3).

Reflections occur when the transmitted wave encounters long objects respect to its wavelength, and part of the wave is absorbed and part reflected. This phenomenon depends on the nature of the wave (polarization, amplitude, etc.) and the impacting material. On the other hand, scatterings occur when the wave pass through several small objects, hence the energy is scattered. Finally, diffraction occurs when sharp edges of objects cause secondary waves, with the property to bend around it. These phenomena cause a wave to travel through multiple paths from the transmitter to the receiver (known as multipath propagation). Consequently, waves can add constructively or destructively, causing fadings or gain points (Rappaport, 2002, chapter 4).

For the reasons mentioned above, indoor propagation models result difficult to develop and in some cases are inaccurate (Lopez et al 2009). For this reason, practical measurements are usually performed. Representing these measurements as a function of position, practical coverage maps are obtained.

Summarizing, to determine the quality of a wireless link there exist several metrics. However, is not clear which one is the best to use. Environments considered for propagation studies are diverse, and due to phenomena such as diffractions, reflections and scattering some models may become too difficult to develop. For this reason, practical measurements are performed and coverage maps are built with them.

In the next section, the Somport Tunnel, the test scenario selected, is described, along with a Ray Tracing propagation model, in order to study phenomena in tunnel environments.

Chapter 3

Test Scenario: The Somport Tunnel

Regarding the test scenario, we chose a special area of interest for University of Zaragoza research group RoPeRT (Robotics, Perception and Real Time): The Somport railway tunnel, which is 7.7 Km long and connects the Spanish city Cancfranc with Pau, in France. At present in this tunnel, RoPeRT is making studies about wireless protocols testing, hostile environment network development, as well as navigation strategies for multi-robot teams under connectivity constrains (Tardioli and Villarroel 2007; Tardioli et al. 2010; Sicignano et al. 2011).

A special area of the tunnel was selected, depicted as “Zone of Interest” in figure 1. This zone is 2.5 Km long and is located between a laboratory (before which the area is traveled by vehicles), and the French frontier; and suffers a change in slope. After getting passed the laboratory, the area is not usually transited, therefore, it becomes of special interest for surveillance purposes, for example, through robots.

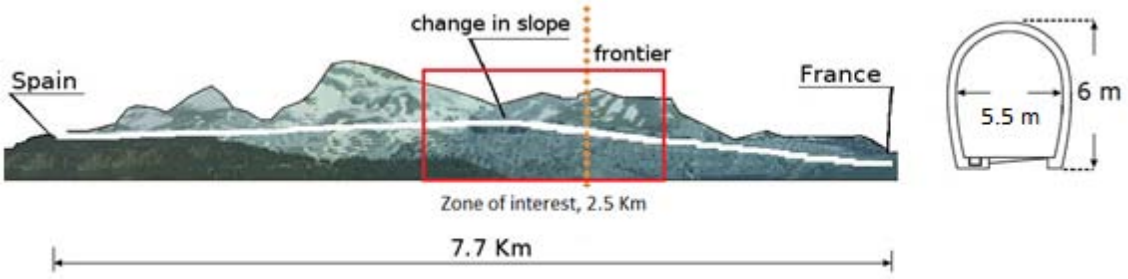

Figure 1. Longitudinal and Cross section of the Somport Tunnel

Other special characteristic of this tunnel is the presence of vaults and galleries, depicted in figure 2. In the Zone of Interest, there are several vaults and two lateral galleries.

(a) (b)

Figure 2. Small Vaults in the tunnel (a), and galleries (b).

Ray Tracing Model

In order to obtain an idea of propagation phenomena and patterns that could be found in the tunnel, we implemented in MATLAB ™ a rectangular straight tunnel Ray Tracing model, developed by Valenzuela (1993) and described later by Kermani and Kamarei (2000) to calculate the average received signal power as a function of position. It is important to highlight the fact that we will not take into account the vaults and galleries of the Somport tunnel for the model, nor the change in slope.

The model considers every wall as a reflective plane (mirror), and takes into account the direct and reflected rays (after a random number of reflections), as well as the angle of incidence and material properties, such as conductivity and permittivity constants.

The first step is to define the rays to compute. In this case, we chose the direct ray, and the rays reflected by the right and left walls. Because of the horseshoe shape of the Somport tunnel, rays reflected in the roof will not be studied.

After defining the rays, a sum of the received power due to direct rays, rays after the first reflection and so on until the last number of reflection, is computed. For each ray, the calculated loss is the Free Space Loss.

According to Kermani and Kamarei (2000), the received power is defined as

$$\Pr = Pt \left\{\frac{\lambda}{4\pi}\right\}^2 \left\{\left|\frac{G_d(x)}{r} + \sum_{i=1}^{N-1} \frac{G_{ri}(x) R_i \exp(j\varphi_i)}{r_i}\right|^2\right\} \qquad (1)$$

Where

Pr = Received power.
Pt = Transmitted power.
λ = Free space wavelength.
G_d = Square root of transmit and receive antenna gain product in Line of Sight (LOS) direction.

G_{ri} = Square root of transmit and receive antenna gain product in direction of *ith* ray.
r = Path length of LOS direction.
r_i = Path length of *ith* ray.
R_i = Reflection coefficient of the *ith* ray.

And,

$$\varphi_i = \frac{2\pi \Delta l_i}{\lambda} \qquad (2)$$

Where Δl_i is the distance between the LOS and the *ith* path.

If the ray is horizontally polarized respect to the surface, the reflection coefficient is given by

$$R_{hi} = \frac{\cos(\varphi_i) - (\varepsilon - sin^2(\varphi_i))^{\frac{1}{2}}}{\cos(\varphi_i) + (\varepsilon - sin^2(\varphi_i))^{\frac{1}{2}}} \qquad (3)$$

In the other hand, if the ray is vertically polarized respect to the surface, the reflection coefficient is given by

$$R_{vi} = \frac{\varepsilon \cos(\varphi_i) - (\varepsilon - sin^2(\varphi_i))^{\frac{1}{2}}}{\varepsilon \cos(\varphi_i) + (\varepsilon - sin^2(\varphi_i))^{\frac{1}{2}}} \qquad (4)$$

Where φ_i is the angle of incidence for the ray, and

$$\varepsilon = \varepsilon_{ri} - j60\sigma_i \lambda_i \qquad (5)$$

Being ε_{ri} and σ_i the relative permittivity and conductivity of the media.

After implementing the algorithm, we made a simulation with the "Zone of Interest" values: 5.5 m wide, 2.5 Km in length, operating frequency of 2.4 GHz. A maximum number of 6 reflections was considered. The relative permittivity ε_r = 5 and relative conductivity σ =0.01 s/m were selected, as values widely used in the literature.

At first it can be seen longitudinal variations, depicted in figure 3 for a transversal distance of three meters from the right wall. The transmitter is located at the beginning (0 m in length), at 3 meters from the right wall, and at 2.5 meters from the left wall.

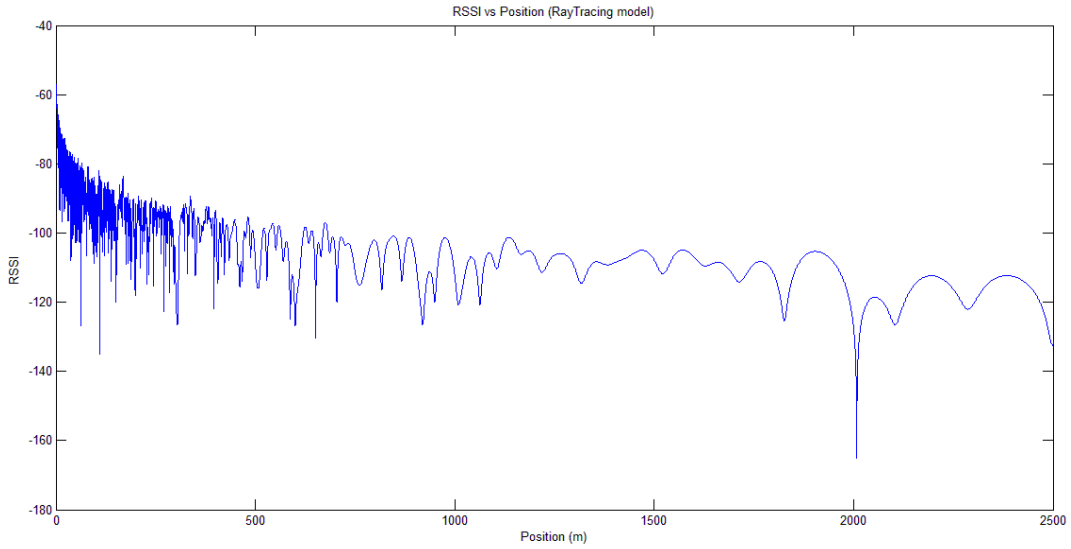

Figure 3. Longitudinal fadings derived from Ray Tracing Model.

During the first 600 meters we can see several narrow fadings. After that area, more notable wider fadings appear. The signal power follows a logarithmic decay.

Regarding the transversal variations, they are illustrated in figure 4 for a longitudinal distance of 1000 m, as an example. The transmitter is located in the same place as in the above example.

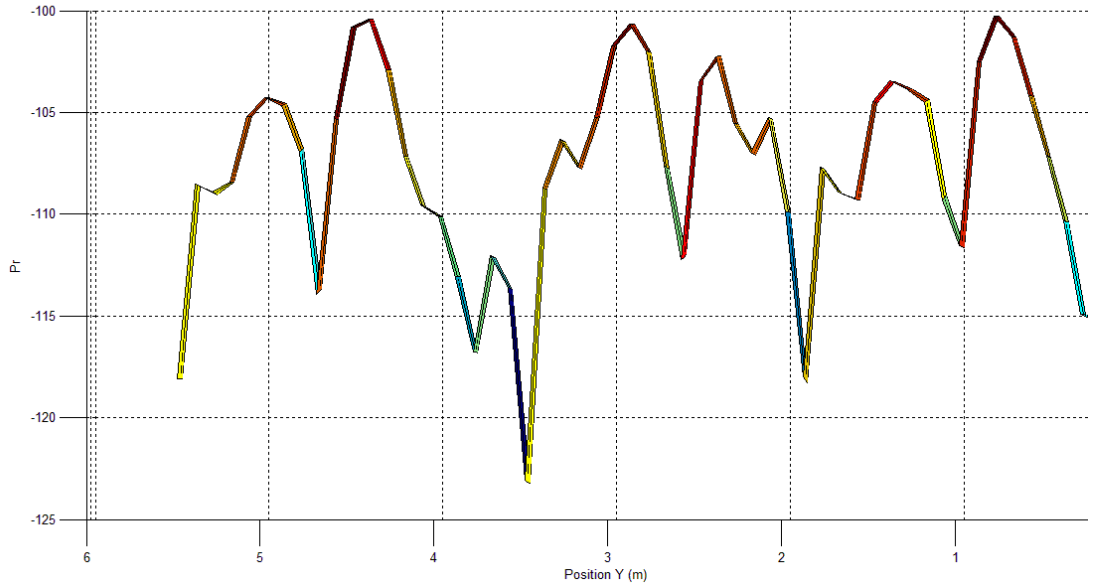

Figure 4. Transversal variation derived from Ray Tracing Model.

It can be observed that cross-section variations are also of great importance, with a difference greater than 20 dB between local maximums and minimums in simulations. This should be taken into account when designing the tools for communication mapping.

Finally, in figure 5, we depict an example in three dimensions, where transversal and longitudinal variations can be observed together within 20 meters in length (X position from 900 to 920 meters from the transmitter). Again, the transmitter is located at 3 meters from the right wall.

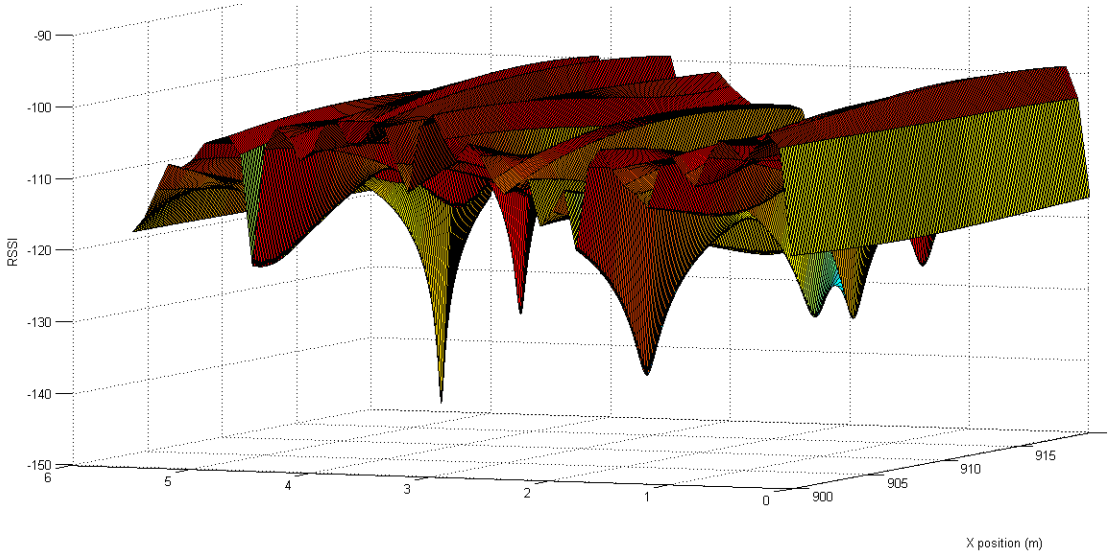

Figure 5. Three Dimensional view for Longitudinal and Transversal variations in tunnels.

In summary, in the case of tunnel scenarios, longitudinal and transversal variations are of great importance, and should be taken into account to design tools for coverage mapping.

In the next section we present the tools developed for creating communication maps, both in a large scale and in a small scale.

Chapter 4

Tool Development for Coverage Map Building

A specific propagation model for the Somport tunnel is not available. In addition, it has galleries, vaults and a change in slope that would hamper the development of one. Therefore, building a coverage map with experimental measurements appears to be the most feasible solution in order to study propagation in this environment.

The atmosphere in the tunnel is hostile: low temperatures, darkness, dust and air currents, which make it difficult for humans to work comfortably. Its length makes it not economically feasible to deploy a sensor network to study propagation phenomena. It seems to be the best option to place sensors on a mobile platform and move it.

There isn´t a physical map of the tunnel available. By building this, we would be able to create the coverage map associated to the real map, as well as determine the effect of vaults and galleries over propagation.

The first goal was to create a large scale coverage map for the “Zone of Interest”. Later, it became necessary to build a model on a smaller scale in certain regions of interest, and a second tool was developed.

4.1 Large Scale Model Tool

The first solution considered was to place wireless sensors over the robotics platforms available in the lab, Pioneer P3AT robots, but due to the length of the tunnel and the speed limit of these robots, it would take a huge amount of time to build the map. For this reason, a real vehicle was used.

Because of its modularity and integration with other solutions for RoPeRT group, it was decided to work on ROS meta-operating systems, which runs over Linux. We developed a communication module, responsible for frame broadcasting, reception and processing. In

order to associate signal quality to position, an odometry module was designed. Navigation is by a human operator for being the case of a real vehicle.

4.1.1 Communication Module

In order to obtain signal quality in certain points we need at least a transmitter and a receiver, as well as a quality metric to represent and analyze.

Regarding the quality metrics, RSSI and PDR were selected. To represent the received power we chose the RSSI, as it's reported by the network card. Because it can be obtained the RSSI of received packets only, we need an additional metric to know how many frames have been received. The PDR was implemented for this purpose, by adding a sequence number in the frame header. Knowing how many packets have been sent and lost, PDR can be computed and used to validate RSSI measurements. Besides, there is a strong correlation between PDR and RSSI, as stated by Vlavianos et al. (2008) and Dhananjay et al. (2003). In this manner, we are combining two metrics to obtain an idea about link reliability and signal quality.

Concerning the hardware, for the emitting node, a PcEngines ALIX3D3 board was selected. It is equipped with an Atheros™ based chipset wireless card, and it's sealed and designed for hostile environment operation. It runs Linux operating system, and was programmed to broadcast frames that later on will be received by a node to be analyzed.

For the receiving node, a laptop running meta-operating system ROS over Linux was chosen, equipped with an Atheros™ network card. "*ROS (Robot Operating System) provides libraries and tools to help software developers create robot applications. It provides hardware abstraction, device drivers, libraries, visualizers, message-passing, package management, and more. ROS is licensed under an open source, BSD license.*" (http://www.ros.org/wiki/).

Previously, a driver was developed to obtain the RSSI and floor noise values from the network card. A ROS executable communicates with the network card to obtain these values, and received power in dBm is computed through the sum of these in the case of Atheros cards (Bardwell 2002). In table 1 can be observed a summary of the main characteristics for both nodes, and they are shown in figure 6.

	Transmitter	Receiver
Model	PcEngines ALIX3D3, Atheros wireless card	Dell Laptop, Intel Core 2 Duo T9300 2.5 GHz Processor, 2 GB RAM memory, Atheros wireless card
Operating System	Linux	ROS over Linux
Working frecuency	2.142 Ghz	
Antenna polarization	Vertical	
Frame size	250 bytes	
Transmission speed	6 Mbps	
Frame periodicity	5 ms	

Table 1. Transmitter and Receiver nodes characteristics.

4.1.2 Odometry Module

To associate signal quality to position, an odometry module was designed.

Regarding the hardware, it's mainly composed by an infrared light emitter-receiver. Reflective tape was placed over the rear wheels. Therefore, we can perceive an electronic pulse each time the tape passes in front of the sensor.

The traveled distance is calculated based on the wheel circumference length, the number of reflective tape bands, and hence the number of received pulses. In figure 6 we can observe the final assembly for this module.

4.1.3 Test Platform

All of these modules were integrated on a real vehicle, in this case, an all terrain.

In order to study transversal variations of the signal we decided to place 3 antennas, located at the ends and center of the vehicle. To avoid the interference the vehicle may cause, a platform was installed in the roof, as observed in figure 6.

Three laptops were used. One is in charge for both odometry and communication modules, while the others are responsible for communication modules only. Data is synchronized through the sequence number in the emitted frames.

Figure 6. Large Scale Tool Modules: Communication module: Transmitter (a) and Receivers (b). Odometry module (c), and antenna platform (d)

4.2 Small Scale Model Tool

With the aim of studying certain zones in more detail, such as the effect of vaults and galleries over propagation, arises the need to build a physical map of the surrounding environment and associate link quality to that map. Because the length in this case is smaller, it's feasible to use Pioneer P3AT robots.

Again, a modular solution was proposed. The communication module is the same as the one described above. Nevertheless, the navigation is not responsibility of a human operator now, and to this end a navigation module was implemented. Finally, to build the environment map, a SLAM (Simultaneous Localization and Mapping) module was used. All of these modules were designed for ROS operating system.

4.2.1 Navigation module

This module is composed by two layers: local navigation and reactive navigation. For the local navigation, an algorithm was developed to plan local goals based on the distance to

the tunnel walls. For reactive navigation, an implementation in ROS of the Dynamic Window Approach, described by Fox et al. (1997), was used, with some minor changes in the objective function.

a) Online goal planning

To obtain a reliable coverage map and make a precise study about transversal variations of the signal, the robot must be able to travel in a straight line, at a constant distance from walls or following the center of the tunnel.

Because of the width of the tunnel is not always constant, as in the case where a vault is found, the algorithm was designed to detect the walls and filter galleries and vaults. The program was structured in 4 phases:

1. Wall Detection: based on the information from a laser scan sensor, a program receives these measurements and, using the Hough Transform, detects the straight lines derived from these. These happen to be the tunnel walls, galleries and vaults.

2. Vault filtering: once the lines are detected, a filtering process is applied to eliminate the small vaults and detect the pair of tunnel walls. This is done with information about the number of votes obtained by the Hough Transform.

3. Goal line: after obtaining the pair of walls, a line is generated in a way that passes through the center of both lines, or at a certain constant distance from the walls. The navigation route converges to this line.

4. Goal setting: once the goal line is determined, a goal is placed over it, at a certain distance from the robot (in the longitudinal dimension). Trigonometric calculations are computed so that the goal is located according the actual robot coordinate system.

This process is repeated every second (f = 1 Hz), a value set in simulations, yielding good results in the real implementation. In this manner, we keep the robot traveling in a straight line along the tunnel. The whole algorithm can be visualized in figure 7.

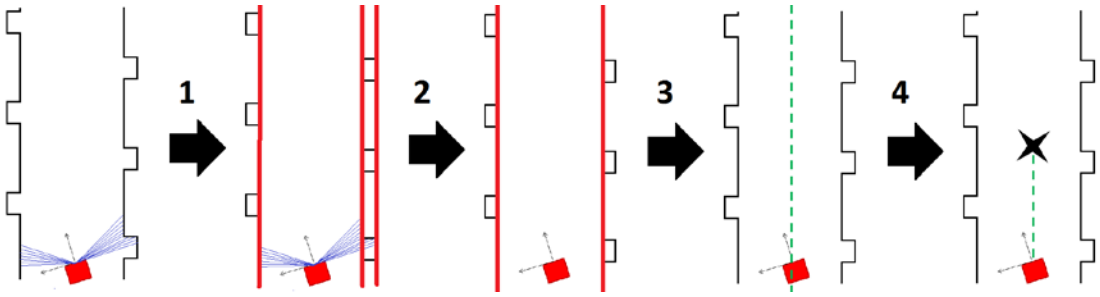

Figure 7. Online goal planning algorithm

b) Reactive navigation

In order to avoid obstacle collision, an implementation of the Dynamic Window Approach (Fox et al. 1997) was used. This approach was considered the most appropriate for this environment because it avoids oscillatory behaviors in corridors or tunnels. This problem appears using the potential field approach, as stated by Fox et al. (2007). Besides, this method considers the vehicle dynamics and is suitable for robots traveling at "high speeds".

The original method describes the procedure to obtain linear and angular speed in two phases:

1. Search space, where possible velocities are defined. These velocities are those which are collision free, and able to be reached within a short interval of time (given the robot accelerations).

2. Optimization, where the objective function

$$G(v, \omega) = \alpha * \text{heading} + \beta * \text{distance} + \gamma * \text{velocity} \qquad (6)$$

Is maximized, being "heading" the orientation of the robot, "distance" the distance to the closest obstacle, and "velocity" the speed of the robot.

For the meta-operating system ROS, there is an implementation of this approach (http://www.ros.org), with a difference in the objective function to maximize. In this case, the function is given by:

$$G(v, \omega) = \alpha * (\text{path}) + \beta * (\text{goal}) + \gamma * (\text{obstacle\_cost}) \qquad (7)$$

Where "path" is the distance to the local navigation route, "goal" is the distance to the local goal, and "obstacle_cost" is a measure about how much the controller should attempt to avoid obstacles.

To determine the best α, β and γ, three values were assigned to each one: high, medium and low. A model of the Pioneer P3AT was tuned in Stage™ and simulations with all 27 possible combinations were made in a corridor scenario. Then, the parameters in the real robot where tuned around simulation results. The values obtained are depicted in table 2.

Parameter	Value
α	0.4
β	0.3
γ	0.03

Table 2. Parameters used for ROS DWA implementation

4.2.2 Teleoperation Module

In order to achieve a semi-autonomous or guided navigation for the robot to be used in other scenarios, the system was equipped with a PS3JOY module (http://www.ros.org), which allows to drive the robot using a commercial PlayStation™ game controller.

4.2.3 SLAM Module

With the purpose of associating signal quality with the position of vaults and galleries, or reference in a better way communication loss risk zones, it would be useful to build a physical map of the environment. To this end, a SLAM (Simultaneous Localization and Mapping) module was implemented in the system.

In a basic sense, SLAM algorithms deal with map representation and the estimation technique (for the actual localization and map creation). A summary of these can be observed in figure 8.

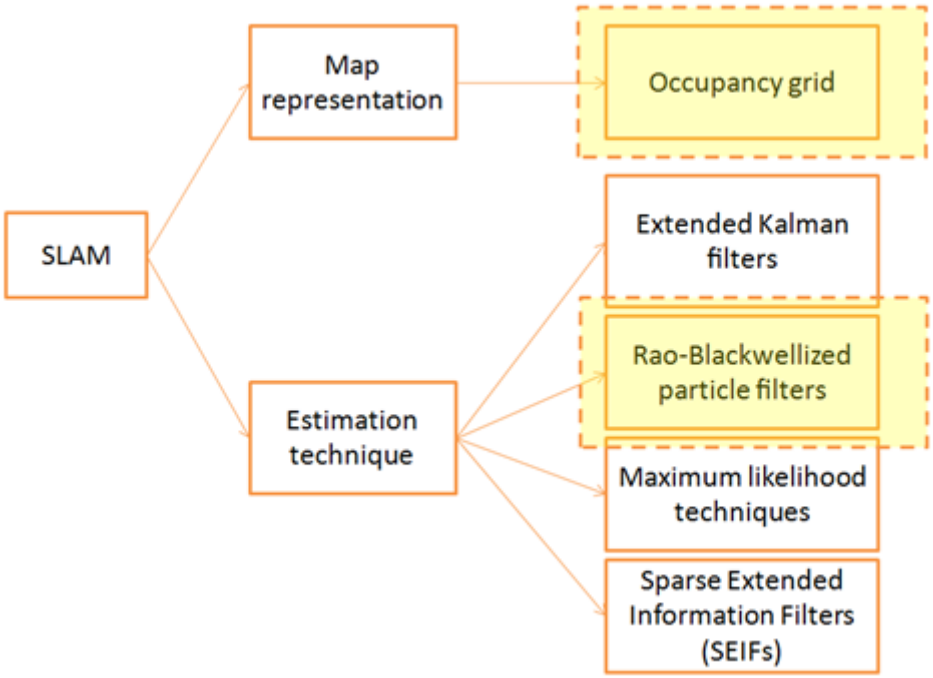

Figure 8. Basic SLAM algorithms structure

Nowadays, algorithms based on particle filters as estimation technique are becoming important. There is an implementation in ROS, called SLAM-gmapping, capable to realize SLAM with this estimation technique. It uses the "Rao-Blackwellized particle filter" approach, described by Grisetti et al. (2005) and Grisetti et al. (2007).

This approach creates the map in 4 phases:

1. Sampling: new particles are generated according to the particles of the previous step and the proposed distribution.
2. Weighting: each particle is weighted according to actual and previous information.
3. Re-sampling: particles (or substitutes) are drawn according to its weight. After this process, all particles weight the same.
4. Map estimation: for each particle a map is estimated, which is processed according to its observation history.

This approach differs from other particle filter approaches in a way that there is no fixed distribution proposal, odometric and other sensor information is added to generate a new set of particles, and more important, re-sampling is not being executed every time, which eliminates the “particle depletion” problem.

4.2.4 Test Platform

As a test platform, a Pioneer P3AT robot was used. We equipped the robot with a robust structure, so it would hold the 3 laptops and antennas at the same height as in the all terrain vehicle. For navigation and mapping purposes, a SICK LMS-200 Laser Measurement Sensor was added. The final assembly can be observed in figure 9.

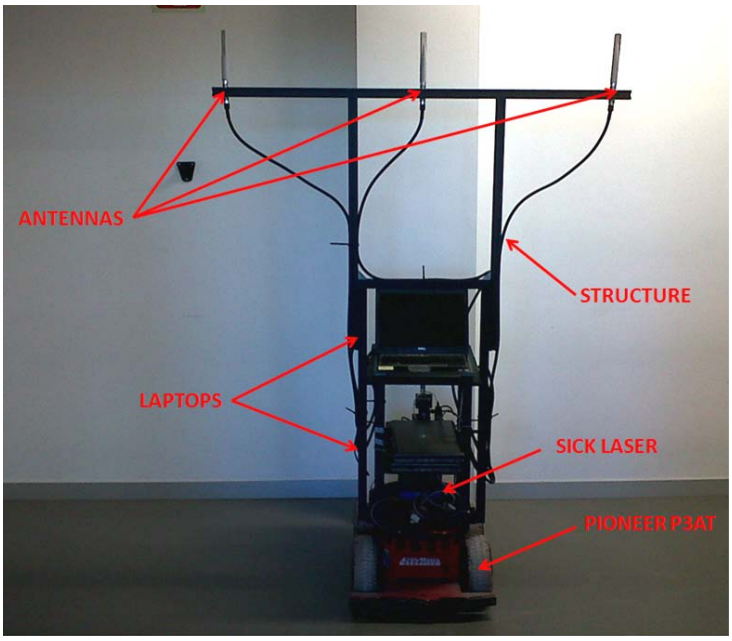

Figure 9. Final assembly for Pioneer P3AT.

Chapter 5

Results

In this section, firstly, we present results obtained from large scale and small scale propagation study in the "Zone of Interest", followed by a comparison between both of them and with the Straight Tunnel Model presented in section 3. From this we derived repeatable phenomena. Later, physical maps of the tunnel obtained by the SLAM module are shown, and with these, vaults and galleries influence over propagation is studied. Finally, transversal variations are analyzed, denoting the importance of spatial diversity, and coverage maps are constructed on this basis.

5.1 Large Scale Model

In order to study how consistent and repeatable propagation phenomena are in the "Zone of Interest" (fadings, gain points, etc), three experiments were performed along the same path, two of them at the same transmission power, and the last one at a lower power.

The path was defined to be the center of the tunnel. First, it was traveled two times (called Journey 1 and 2 for reference purposes) at an average speed of about 8 m/s. The transmission power was selected to be 1 dBm. Travelling at this speed, an approximate of three samples were collected in a wavelength distance (λ=12.5 cm), obtaining 24 samples per meter. Graphs obtained after filtering the signal with a 3rd order Savitzky–Golay filter, 41 samples window size, are shown in figure 10. From now on, three signals will be represented per plot (in different colors), corresponding to the three antennas.

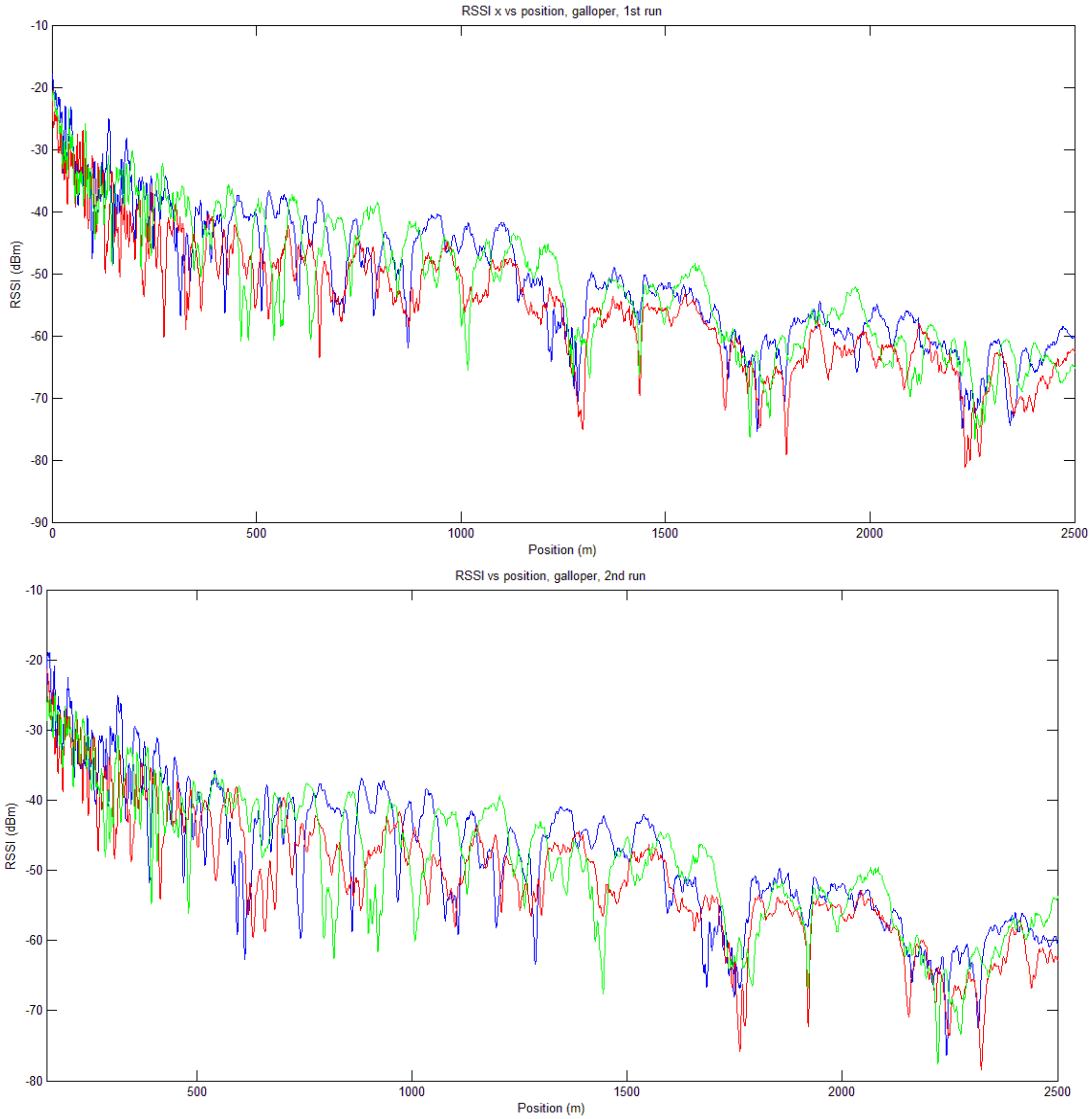

Figure 10. RSSI (dBm) vs Position (m). Journey 1 and 2. PTx=1dBm.

And the PDRs obtained are depicted in table 3.

	Antenna	PDR
Journey 1	b	99,93
	c	99,86
	d	99,95
Journey 2	b	99,97
	c	97,04
	d	96,69

Table 3. PDR for Journey 1 and 2

From these values, it can be noticed that a large amount of packets sent were correctly received (more than 96% in the worst case), so RSSI measurements presented are considered to be reliable.

Both graphs appear to have the same pattern and the same mean values at beginning and the end of the path (25 and 60 dBm respectively). Also, it can be noticed that in the first kilometer several narrow fadings appear, as in the case of simulations for the first 600 meters. After that, wider fadings take place.

For the third experiment, we traveled the same path but with a transmission power 20 dB less than in the first experiment. Received power is depicted in figure 11.

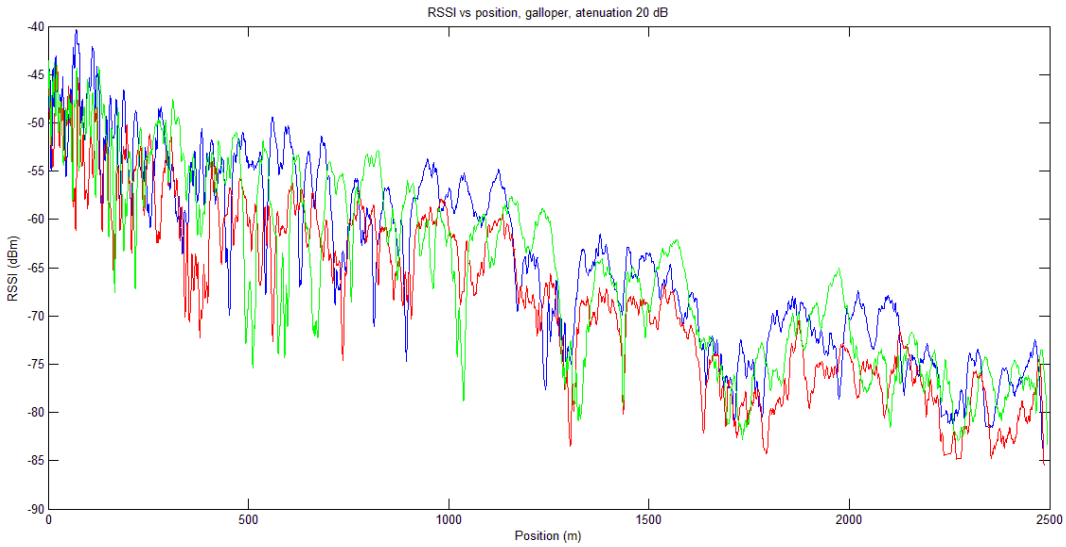

Figure 11. RSSI (dBm) vs Position (m). Journey 3. PTx=-19dBm.

And PDRs obtained depicted in table 4.

	Antenna	PDR
Journey 3	b	98,86
	c	91,79
	d	92,79

Table 4. PDR for Journey 3

This time, PDRs obtained were less than in the previous case. Nevertheless, in the worst case it was greater than 91%. Again, values obtained are considered reliable.

Also, the graph appears to have the same pattern than the previous. In this case, mean values at beginning and the end of the Journey were 43 and 80 dBm respectively, which coincides with the 20 dB attenuator introduced. Later on, these graphs will be compared with the small scale model and the Straight Tunnel model.

In every case, it can be noticed that important wider fadings appear after the first kilometer. To make a more detailed analysis of this area, the small scale model tool (Pioneer P3AT) was used.

5.2 Small Scale Model

In this case, the study area is reduced even more, from the first to the second kilometer in the “Zone of Interest”. This will be called “Fadings Zone”, and can be visualized in figure 12.

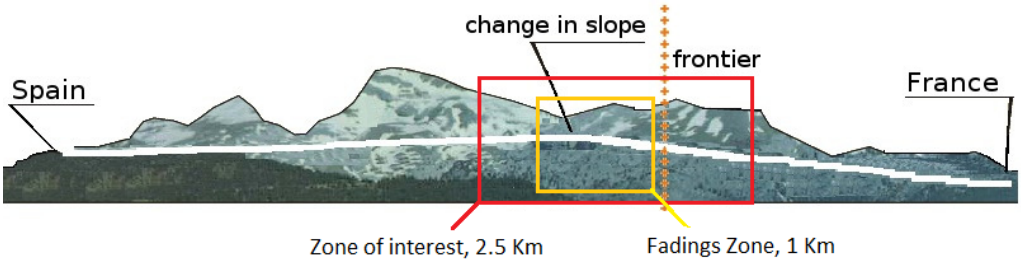

Figure 12. “Zone of Interest” and ”Fadings Zone”.

To study phenomena repeatability, two experiments were performed along the same path as above, in order to compare results with previous ones.

The area was traveled two times (Journey 4 and 5), at an average speed of about 0.6 m/s. The transmission power was selected to be 1 dBm. This time, approximately 41 samples were collected in a wavelength distance (λ=12.5 cm), which represents a total number of 328 samples per meter. Graphs obtained after filtering the signal with a 3rd order Savitzky–Golay filter, 41 samples window size, are shown in figure 13.

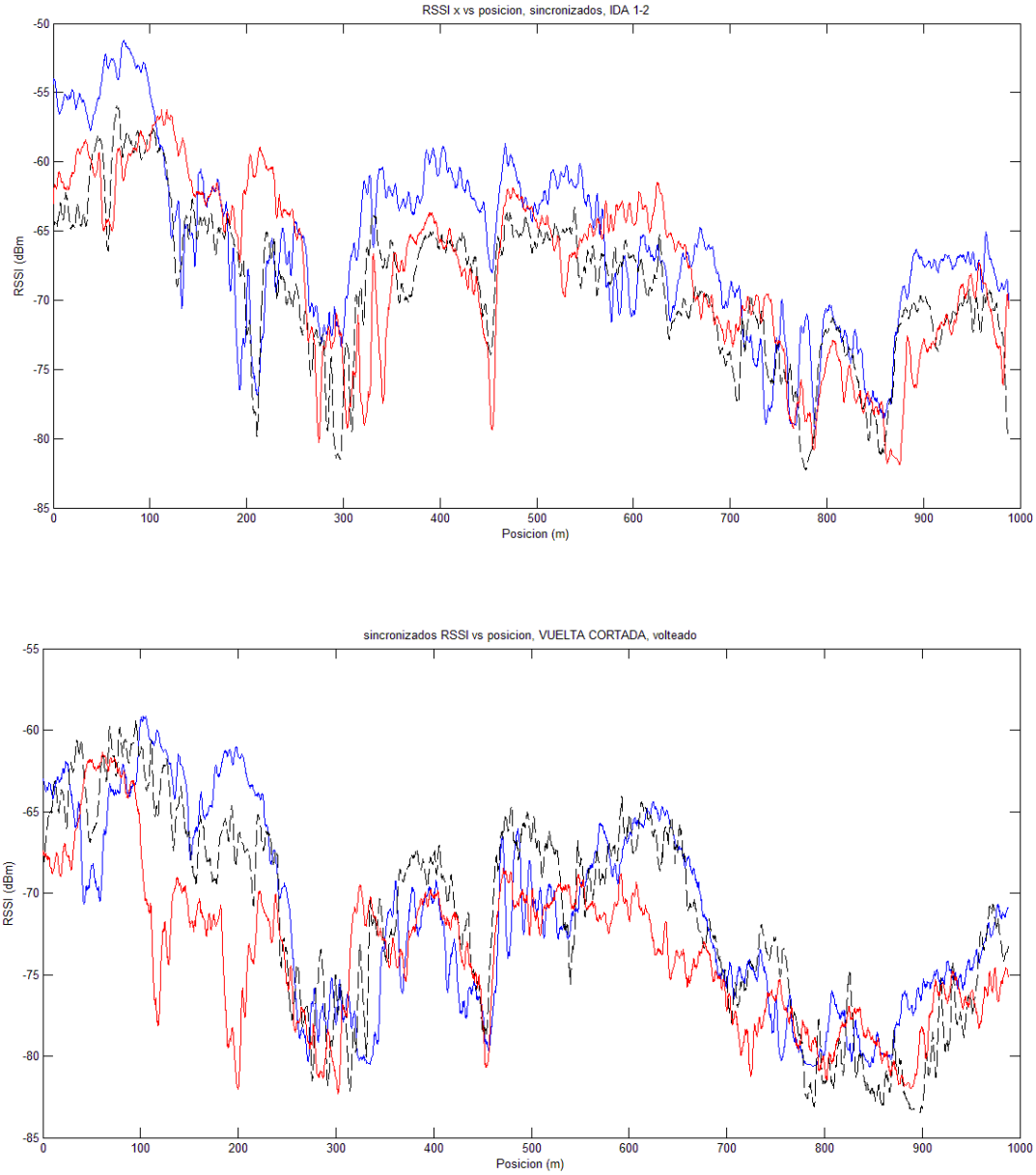

Figure 13. RSSI (dBm) vs Position (m). Journey 4 and 5. PTx=1 dBm.

And the PDRs obtained represented in table 5.

	Antenna	PDR
Recorrido 4	b	98,54
	c	97,49
	d	97,94
Recorrido 5	b	95,69
	c	97,57
	d	97,63

Table 5. PDR for Journey 4 and 5.

For these experiments, the worst PDR obtained was greater than 95%, which gives a high degree of reliability for measurements presented.

Again, both graphs appear to have the same pattern, but in this case we obtained a difference less than 5 dB between both Journeys. In the next section, a comparison on the "Fadings Zone" between all experiments conducted will be performed.

5.3 Comparison between Models

Representing the fading zone for all Journeys (1 to 5) and the Straight Tunnel Model, figure 14 is obtained.

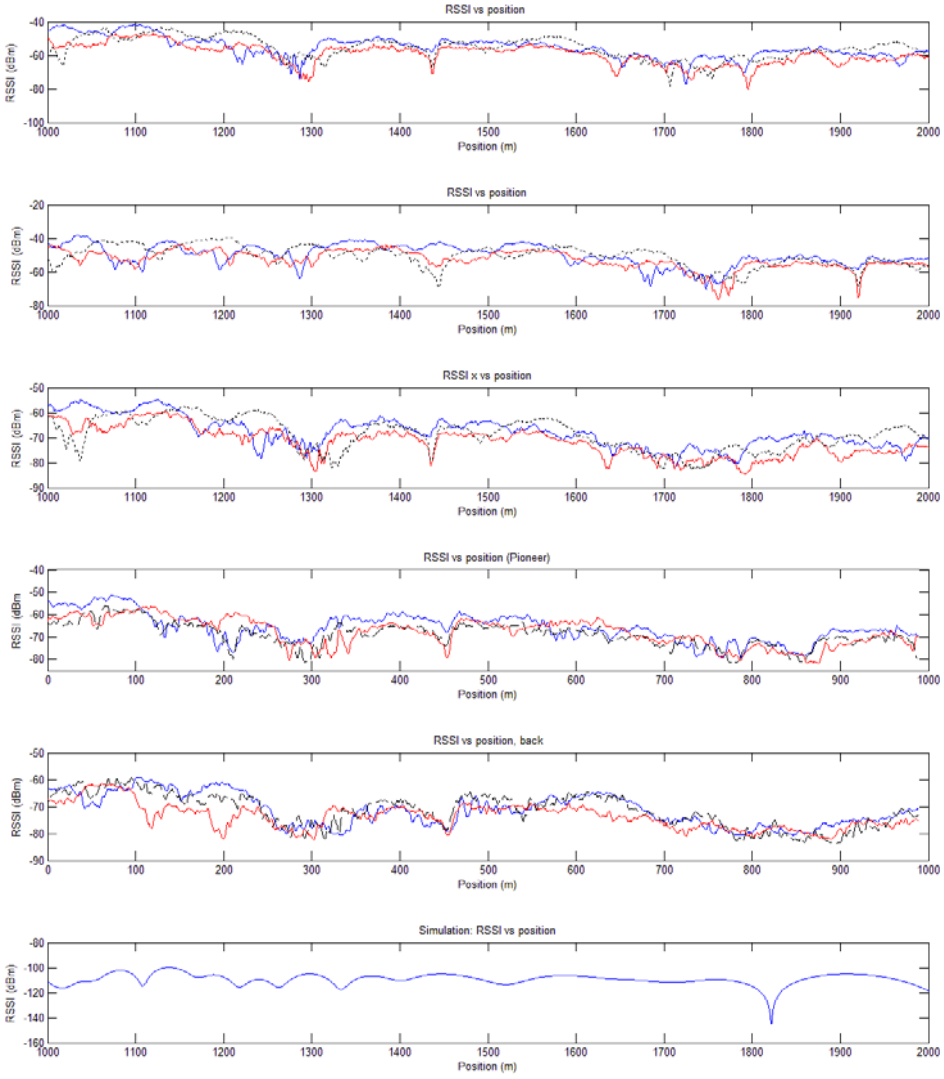

Figure 14. RSSI (dBm) vs Position (m). Journeys 1 to 5, and Ray-Tracing model.

Qualitatively, it can be observed the same pattern in all experiments conducted. In this study, we will remark repeatable phenomena and not the differences between the models (for example, highlighting repeatable fadings and not all of them). For instance, it can be noticed a

considerable fading in all models. In the experiments performed, this fading is located around 1450 m from the transmitter, while in the model implemented in section 3 with the Somport Tunnel values, it's located at 1850 m. However, this model includes direct LOS between transmitter and receiver, a condition not fulfilled in this "Zone of Interest". Also, vertical reflections, vaults and galleries were ignored. Hence the importance of creating an experimental coverage map.

Other phenomenon observed in the experiments but not in the Ray Tracing model is two zones, composed of two fadings each. These fadings have a separation between them of about 75 to 100 m. The zones are located around 1300 and 1700 m respectively. In figure 15 we depict these phenomena for Journey 1 and 4, in order to demonstrate that it appears on both large scale and small scale models. The notable fading that appears in both plots of figure 15 is the fading explained above (located at 1450 m). Complete analysis about all Journeys is presented in Appendix A.

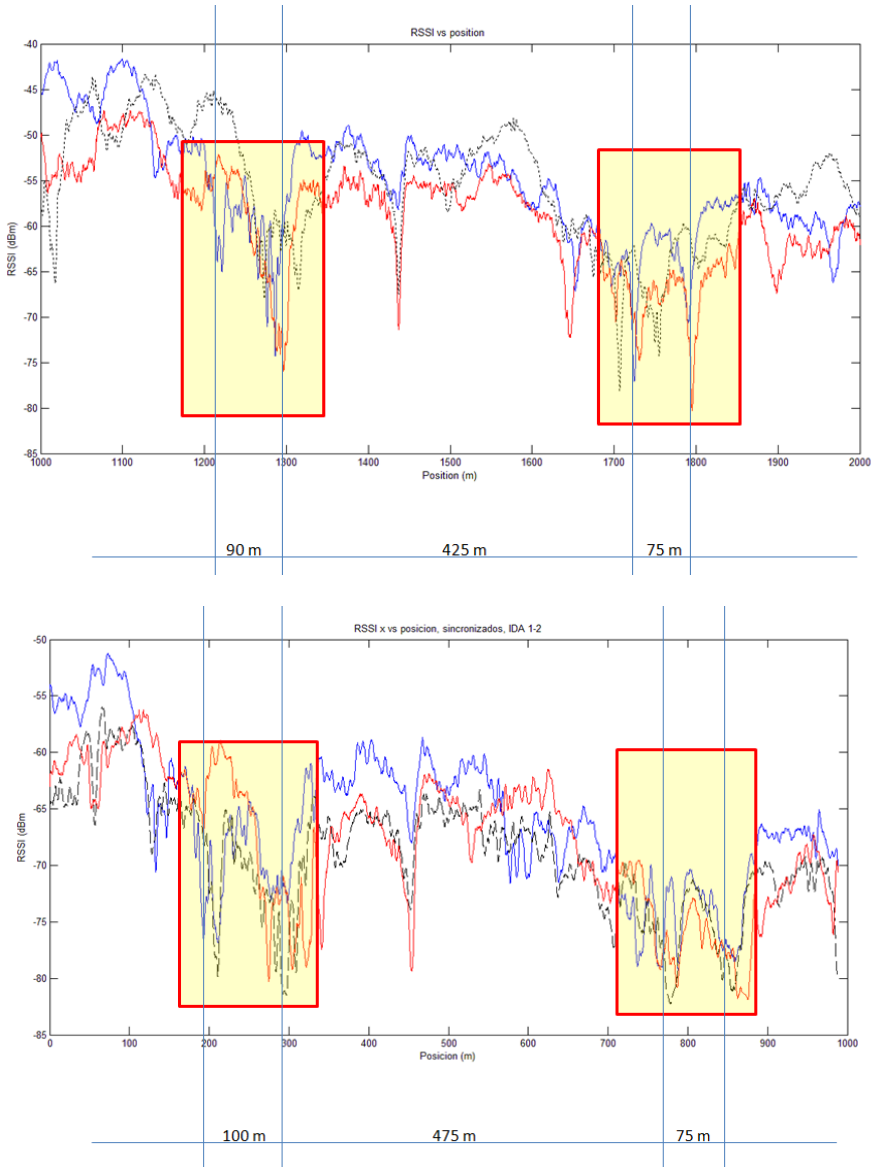

Figure 15. RSSI (dBm) vs Position (m). Repeatable fadings location for Large Scale and Small Scale models.

5.4 Maps Obtained

Because of processing and storage space limitations, SLAM module couldn't be used online in the whole Journey, so Laser and Odometry data was recorded while navigating through the "Fadings Zone" and then, the SLAM algorithm was ran offline with these measurements. Maps obtained for the first and second half of this zone are presented in figure 16. They are depicted in a bigger scale in Appendix E, where vaults and galleries can be appreciated in a better way.

(a)

(b)

Figure 16. First 500 meters of the Fadings Zone (a), and Last 500 m of this zone (b)

And in table 6, data obtained from both Odometry and Maps are compared

	In Fadings Zone
Robot's Travel Time (sec)	1549
Robot´s Avarage Speed (m/s)	0.64
Odometry Map Length (m)	**988**
SLAM obtained Map Length (m)	**1013**
Error	**25 meters ; 2.46%**

Table 6. Odometric vs Obtained Maps data.

Odometry data is used to associate RSSI values to position. SLAM maps obtained are used to associate this data to the real physical map. It can be seen a difference of about 25 meters (over the 1000 meters traveled) between the robot's odometry and the maps, which represents an approximate error of about 2.5%, not very significant for our referencing purposes.

5.5 Influence of vaults and galleries over propagation

Once the maps were obtained, we analyzed the influence of vaults and galleries over propagation, if any. By matching the map with signal quality as a function of position and highlighting the place where small vaults take place (for one antenna in the second half of the "Fadings Zone"), figure 17 is obtained.

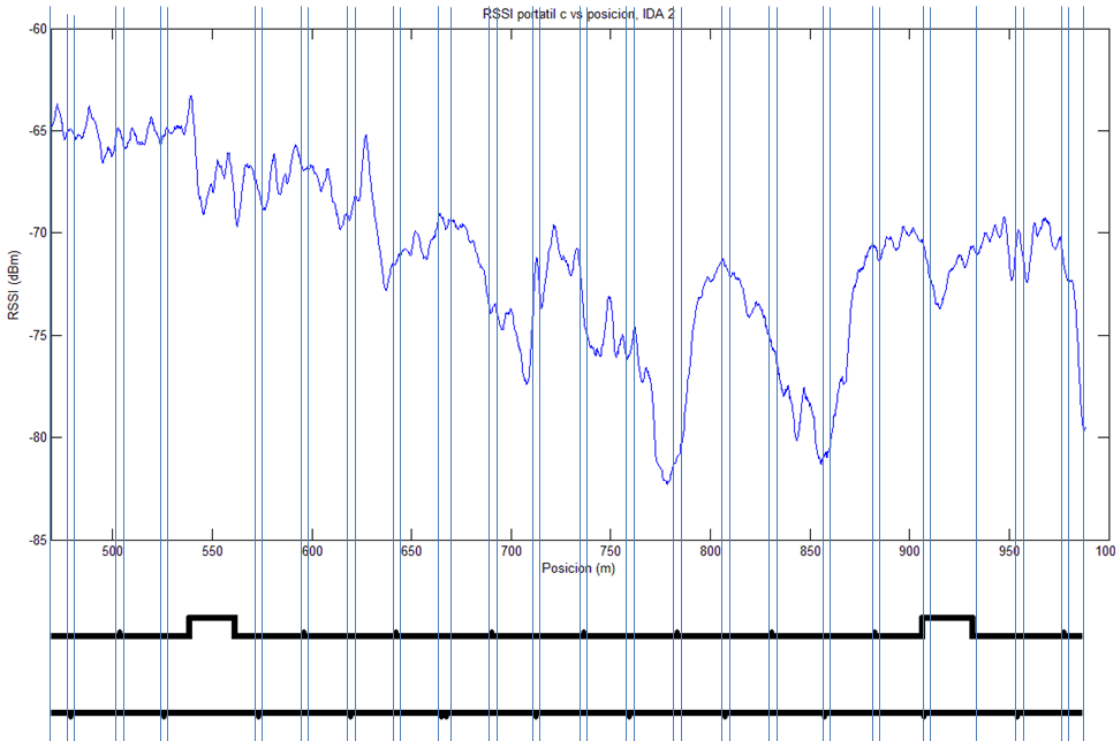

Figure 17. Influence of vaults over propagation in the second half of the fading Zone.

Remaining antennas are shown in Appendix B for the whole Journey. In this case, it's difficult to define a clear influence pattern. No evident fading or gain point can be seen due to vaults. This may be because antennas were placed at 2 meters in height, while vaults are only 1.5 meters high. Analysis varying antenna height is left as a future work. In this case, results serve to dismiss a significant effect of vaults over propagation.

Similarly, by matching galleries location with signal quality as a function of position for two antennas, we obtained figure 18.

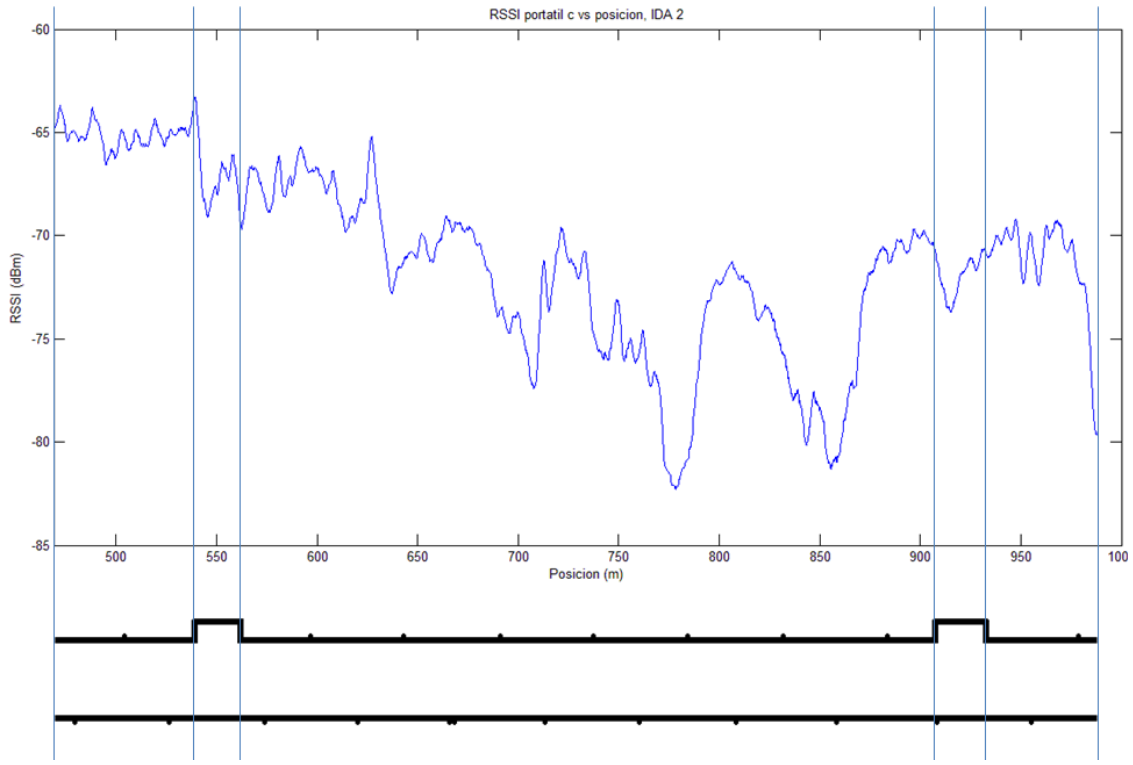

(a)

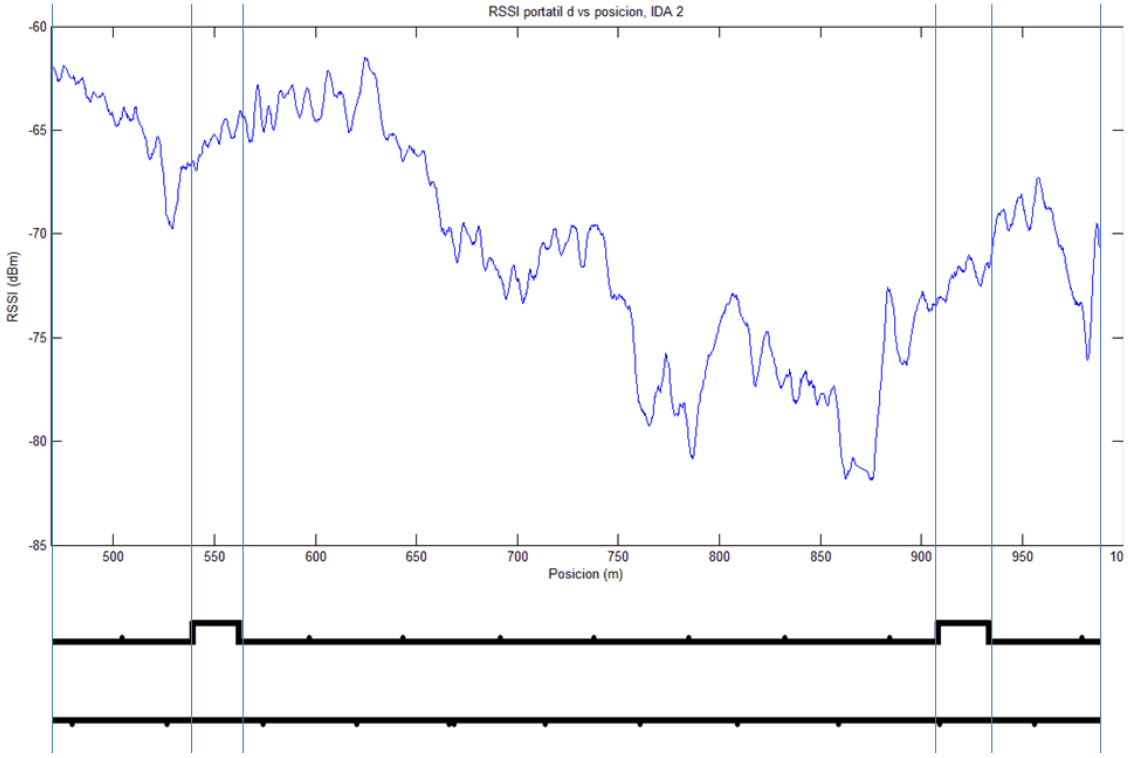

(b)

Figure 18. Influence of galleries over antenna A (a) and antenna B (b) in the second half of the Fadings Zone.

Remaining antennas are shown in Appendix C for the whole Journey. In figure 18 (a), it can be seen a 4 dB attenuation where the galleries take place. Nevertheless, this occurred only for one of the three antennas, so results are not conclusive as to associate these attenuations to the galleries.

5.6 Spatial Diversity Analysis

Spatial diversity is one mechanism or technique used in communication systems with the aim of overcoming multipath propagation distortions. It consists on placing multiple antennas on the receiver, strategically spaced between them. The idea is to select the antenna with the best signal at any time (Rappaport, 2002, chapter 6).

Commercially, there are solutions available to apply this type of mechanisms, for example, to routers or WiFi repeaters. According to or product review, antennas are separated from millimeters, up to a wavelength distance (which is 12.5 cm for 2.4 GHz devices). In figure 19 we depict one commercial antenna array for applying spatial diversity to a WiFi repeater.

Figure 19. Commercial application for antenna diversity.

Nevertheless, in the model developed in section 3, it can be seen that in order to obtain a good quality signal, separation between antennas must be greater than commercial cards diversity systems. In the transversal section depicted in figure 3, we can notice that the distance between a local maximum and a minimum is at least 50 centimeters. Hence, spatial diversity should be in that order of distance. This is the reason why a diversity of about 60 cm was considered.

In figure 20 we depict the received power for the three antennas in the whole “Fadings Zone” (Journey 4), in order to denote the RSSI difference between all of them.

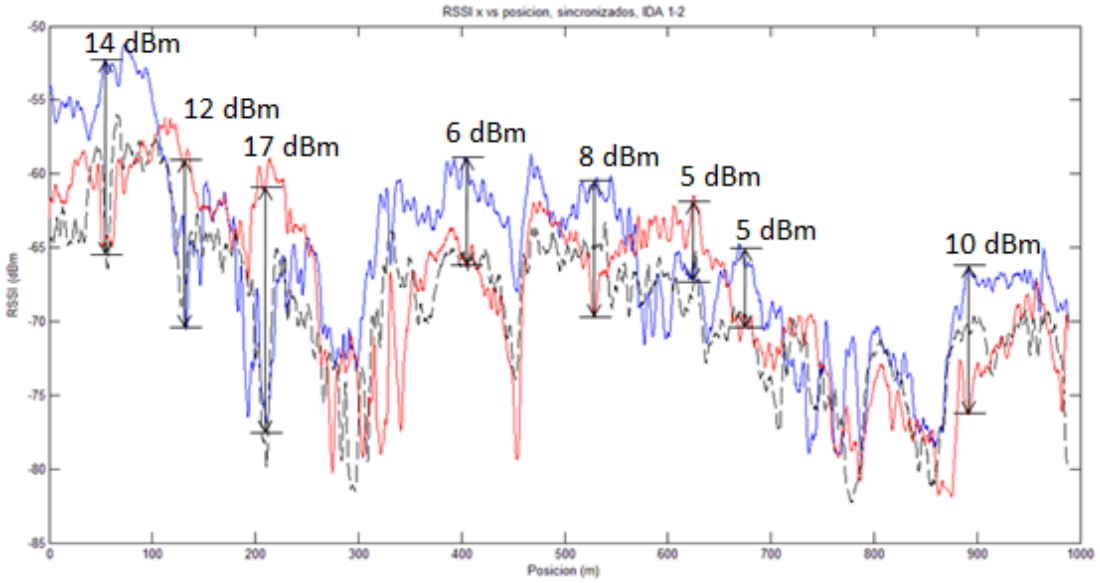

Figure 20. Received power for each antenna in the 4th Journey and differences between them.

It can be seen areas where the difference is up to 17 dBm, which may break a wireless link and cause communication loss, for example, with a base station.

On this basis, we proceed to build a coverage map for this section of interest. At first, signal is discretized in intervals depending on its quality, and a color is assigned according to it so to get a visual appreciation of the hazardous areas in terms of position. This can be seen in figure 21.

Figure 21. RSSI scale for coverage maps.

Firstly, we build a coverage map taking the RSSI measurements from one antenna in the second half in the Fadings Zone. Map obtained is depicted in figure 22.

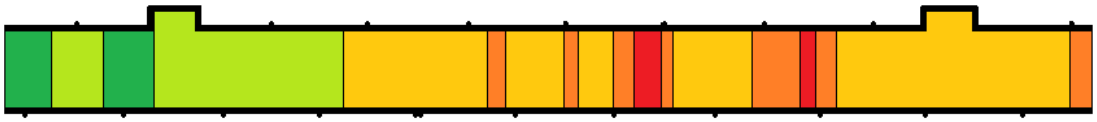

Figure 22. Coverage map for one antenna.

Later, a coverage map taking into account spatial diversity was built; this is, taking the best value among the three signals. Map is depicted in figure 23.

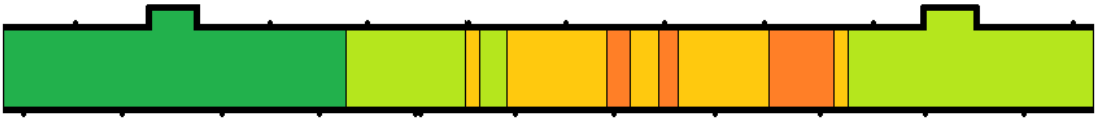

Figure 23. Coverage map with Spatial Diversity.

It's clearly evident the importance of spatial diversity. In our study, we can assert that when applying a spatial diversity in the order of 60 cm (almost 5 wavelengths distance) there aren't hazardous zones (represented in red in the maps), and dangerous zones can be converted into safer regions. However, a more detailed study about diversity must be performed in order to determine the optimal distance between antennas.

The full map for the Fadings Zone is presented in Appendix D.

Conclusions

In this work we have developed tools that allow study of propagation phenomena at a large and small scale.

In the large scale case, odometry and communication modules for meta-operating system ROS were developed, and then implemented on a real all-terrain vehicle.

For small scale maps, communication, navigation and SLAM modules were implemented on a Pioneer P3AT robot. For navigation, due to the peculiarity of the environment, we developed an algorithm based on Hough Transform. This would allow autonomous navigation in straight lines at a constant distance from walls in any parallel wall environment, such as corridors and tunnels.

Because of the modularity of the solution, it can be easily improved by adding modules or upgrading the existing ones. Also, it can be easily migrated to other type of solutions with minor changes.

Both tools were tested in a real environment, an area of interest in the Somport railway tunnel. There is no specific model for this tunnel, and has some features that could hinder the development of one.

A large and small scale models based on measurements were obtained and then compared to a Straight Tunnel Ray-Tracing model, obtaining similarities and differences. First, an important fading was found in all maps. In the case of the built maps, at 1450 meters, while in the model appears at 1820 meters.

Using our tools we also discovered a pattern of two fadings, separated approximately 100 meters. This pattern appears again 400 meters away from its first appearance. This phenomenon is not reported by the Ray-Tracing model, and may be due to all dismissed information when implementing the model (such as ignoring vertical reflections, vaults and galleries), or more important, by implementing a Line Of Sight model when in the tunnel this condition was not fulfilled. In any case, the model was implemented only to obtain an idea about what phenomena to find.

With the aid of physical map building, we were able to dismiss any significant influence of vaults and galleries over propagation.

Also, we noticed the importance of spatial diversity in this type of environments. It was found that with a spatial diversity far beyond commercial network cards (60 cm between antennas), good quality signal can be obtained and communication loss hazardous zones can be avoided in the studied area.

Finally, repeatability of phenomena, an issue that has not been significantly addressed in the revised literature, was proved by performing different types of experiment, with different tools, in different days, and at different transmission powers, obtaining similar results from all of them.

As a general conclusion, we can assert that when involving robotics and communications in tunnel environments, either for surveillance purposes, propagation studies, hostile areas exploration and so on, both transversal and longitudinal variations of signal quality must be taken into account. Regarding diversity, we demonstrated that when applying a “big scale” spatial diversity (beyond commercial network cards diversity), signal quality can be significantly improved in the studied scenario. Finally, coverage maps can help to have an overall idea about propagation in the environment, easily and visually, with not many details. Repeatability of propagation was demonstrated; hence, coverage maps obtained can be useful for several situations.

Future Work

In order to generalize the results of propagation phenomena discovered in this work with the aim of testing different communication protocols, we want to analyze the influence of packet size over tests performed. To do so, other quality metrics should be explored.

Regarding diversity, a more detailed study should be done in order to determine the optimal distance between antennas, with the aim of obtaining the best signal quality possible.

Also, we want to study the occurrence of these phenomena when displacing both transmitter and receiver, so as to use results in multi-robot navigation algorithms under connectivity constrains.

Sicignano et al. (2011) deployed a wireless network in the Somport Tunnel with the aim of testing a novel network protocol. To locate repeaters, RSSI was monitored and when detecting a fading, a node was placed, without taking into account transversal variations. Coverage maps obtained in this work, such as phenomena discovered, could be taken into account in order to deploy the network in a more efficient way.

References

Alonso, J.; Capdevila, S.; Izquierdo, B.; Romeu, J. (2008); “Propagation measurements and simulations in tunnel environment at 5.8GHz”, IEEE Antennas and Propagation Society International Symposium, pp. 1 – 4.

Alonso, J.; Izquierdo, B.; Romeu, J. (2009); “Break point analysis and modelling in subway tunnels”, 3rd European Conference on Antennas and Propagation, pp. 3254 – 3258.

Bardwell,Joe (2002); "Converting Signal Strength Percentage to dBm Values".

Borenovic, M.N.; Neskovic, A.M. (2009.); “Comparative analysis of RSSI, SNR and Noise level parameters applicability for WLAN positioning purposes”, EUROCON 2009, pp. 1895 – 1900.

Dhananjay LaI; Manjeshwar, A.; Herrmann, F.; Uysal-Biyikoglu, E.; Keshavarzian, A. (2003); “Measurement and characterization of link quality metrics in energy constrained wireless sensor networks”, IEEE Global Telecommunications Conference, vol. 1, pp. 446-452.

El-Sayed, H.; Zeadally, S.; Boulmalf, M. (2008); “Experimental Evaluation and Characterization of Long-Distance 802.11g Links”, in Seventh International Conference on Networking, pp. 511 – 516.

Fox, D.; Burgard, W. and Thrun, S. (1997); "The dynamic window approach to collision avoidance", IEEE Robot. Automat. Mag., vol. 4, pp. 23-33.

Grisetti, G.; Stachniss, C.; Burgard, W. (2005); “Improving Grid-based SLAM with Rao-Blackwellized Particle Filters by Adaptive Proposals and Selective Resampling”, Proceedings of the 2005 IEEE International Conference on Robotics and Automation, pp. 2432 – 2437.

Grisetti, G.; Stachniss, C.; Burgard, W. (2007); “Improved Techniques for Grid Mapping With Rao-Blackwellized Particle Filters”, IEEE Transactions on Robotics, Vol. 23 , Issue: 1 , pp. 34 – 46.

Hidayab, M.; Ali, A.H.; Azmi, K.B.A. (2009); “Wifi signal propagation at 2.4 GHz”, Asia Pacific Microwave Conference, pp. 528 – 531.

Holland, M.M.; Aures, R.G.; Heinzelman, W.B. (2006); “Experimental investigation of radio performance in wireless sensor networks”, 2nd IEEE Workshop on Wireless Mesh Networks, pp. 140 – 150.

Howard, A; Siddiqi, S., and Sukhatme, G..(2003); "An Experimental Study of Localization Using Wireless Ethernet". In Proceedings of the International Conference on Field and Service Robotics (FSR).

Karia, D.C.; Lande, B.K.; Daruwala, R.D. (2010); “Radio Channel Characterization for IEEE 802.11”, 2010 International Conference onIntelligent Systems, Modelling and Simulation, pp. 368 – 373.

Kermani, M.H.; Kamarei, M. (2000), “A ray-tracing method for predicting delay spread in tunnel environments”, IEEE International Conference on Personal Wireless Communications, pp. 538 – 542.

López, J; Álvarez, M.; Cacho, M; Paz, E. and Pérez, D. (2009); “Creating wireless coverage maps for mobile robot applications”, X Workshop en Agentes Físicos (Cáceres, Spain), pp:17-25.

Lun-Wu Yeh; Ming-Shiou Hsu; Yueh-Feng Lee; Yu-Chee Tseng (2009); “Indoor localization: Automatically constructing today's radio map by iRobot and RFIDs”, IEEE Sensors, pp. 1463 – 1466.

Matellán, V.;,Cañas, J.M; Serrano, O (2006); “WiFi localization methods for autonomous robots”, Robotica (Cambridge University Press),Vol. 24, Issue 4, pp. 455-461.

Ocana, M.; Bergasa, L.M.; Sotelo, M.A; Nuevo, J.; Flores, R. (2005); “Indoor Robot Localization System Using WiFi Signal Measure and Minimizing Calibration Effort”, Proceedings of the IEEE International Symposium on Industrial Electronics, Vol. 4 , pp. 1545 – 1550.

Oka, A.; Lampe, L. (2010); “Distributed target tracking using signal strength measurements by a wireless sensor network”, IEEE Journal on Selected Areas in Communications, Vol. 28 , Issue: 7, pp. 1006 – 1015.

Rappaport, T. S (2002); “Wireless communications principles and practices”, Chapter 3, Prentice-Hall.

Rong-Hou Wu; Yang-Han Lee; Hsien-Wei Tseng; Yih-Guang Jan; Ming-Hsueh Chuang (2008); “Study of characteristics of RSSI signal”, . IEEE International Conference on Industrial Technology, pp. 1-3.

Sicignano, D.; Tardioli, D.; Cabrero, S. and Villarroel, J. L. (2011); “Real-Time Wireless Multi-Hop protocol in Underground Voice Communication”, Ad Hoc Networks, ISSN 1570-8705

Tao Liu; Kamthe, A.; Lun Jiang; Cerpa, A. (2009); “Performance Evaluation of Link Quality Estimation Metrics for Static Multihop Wireless Sensor Networks”, 6th Annual IEEE Communications Society Conference on Sensor, Mesh and Ad Hoc Communications and Networks, pp. 1-9.

Tardioli, D. and Villarroel, J. (2007); “Real Time communications over 802.11 : RT-WMP”. The Fourth IEEE International Conference on Mobile Ad-hoc and Sensor Systems (MASS ’07).

D. Tardioli, A.R. Mosteo, L. Riazuelo, J.L. Villarroel, L. Montano (2010); “Enforcing network connectivity in robot team missions”, The International Journal of Robotics Research, vol. 29, pp. 460-480.

Vlavianos, A.; Law, L.K.; Broustis, I.; Krishnamurthy, S.V.; Faloutsos, M. (2008); “Assessing link quality in IEEE 802.11 Wireless Networks: Which is the right metric?”, in IEEE 19th International Symposium on Personal, Indoor and Mobile Radio Communications, pp. 1 – 6.

Wapf, A.; Souryal, M.R. (2009) “Measuring Indoor Mobile Wireless Link Quality”, IEEE International Conference on Communications, pp. 1-6.

Wu, D.; Djukic, P.; Mohapatra, P. (2008), “Determining 802.11 link quality with passive measurements”, IEEE International Symposium on Wireless Communication Systems, pp. 728 – 732.

Xinrong Li (2006); “RSS-Based Location Estimation with Unknown Pathloss Model”, IEEE Transactions on Wireless Communications, Vol. 5 , Issue: 12 , `pp. 3626 – 3633.

Zhang, Y.P.; Hwang, Y.; Kouyoumjian, R.G. (1998); “Ray-optical prediction of radio-wave propagation characteristics in tunnel environments. 2. Analysis and measurements”, IEEE Transactions on Antennas and Propagation, vol. 46, issue 9, pp. 1337 – 1345.

Zvanovec, S. ; Pechac, P. ; Klepal, M. (2003); “Wireless LAN Networks Design: Site Survey or Propagation Modeling?” Radioengineering, vol. 12, no. 4, pp. 42-49.

Appendix A: Repeatable Fadings in the "Fadings Zone"

As stated in the work, we will focus on repeatable phenomena and not the differences between the models. As mentioned, a repeatable phenomenon of two zones, composed of two fadings each, was found. Below, we denoted these zones for each antenna where it was more evident, Journey 1, 3 and 4, followed by a summary table with all data respect these fadings.

For each Journey, a total of three antennas were analyzed (ANTENNA A, B and C respectively).

JOURNEY 1

Antenna A:

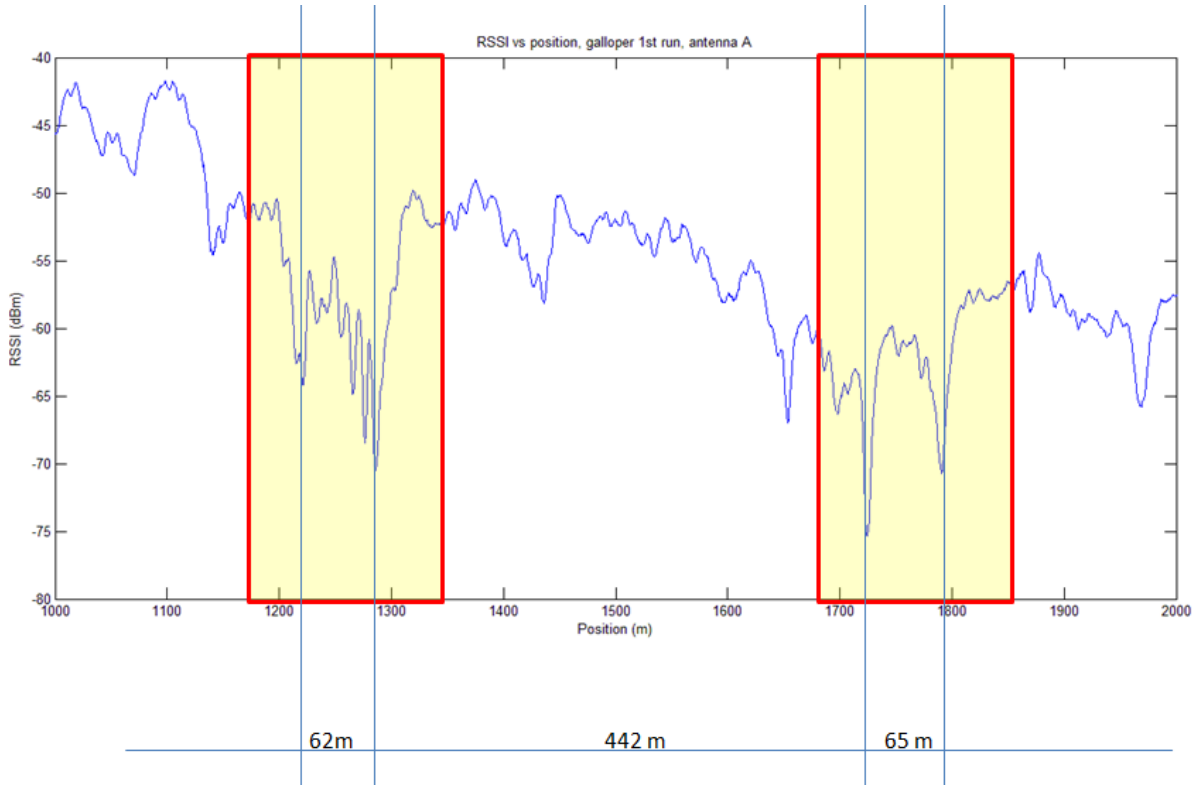

Figure A1. Repeatable fadings for Antenna A in Journey 1.

Antenna B:

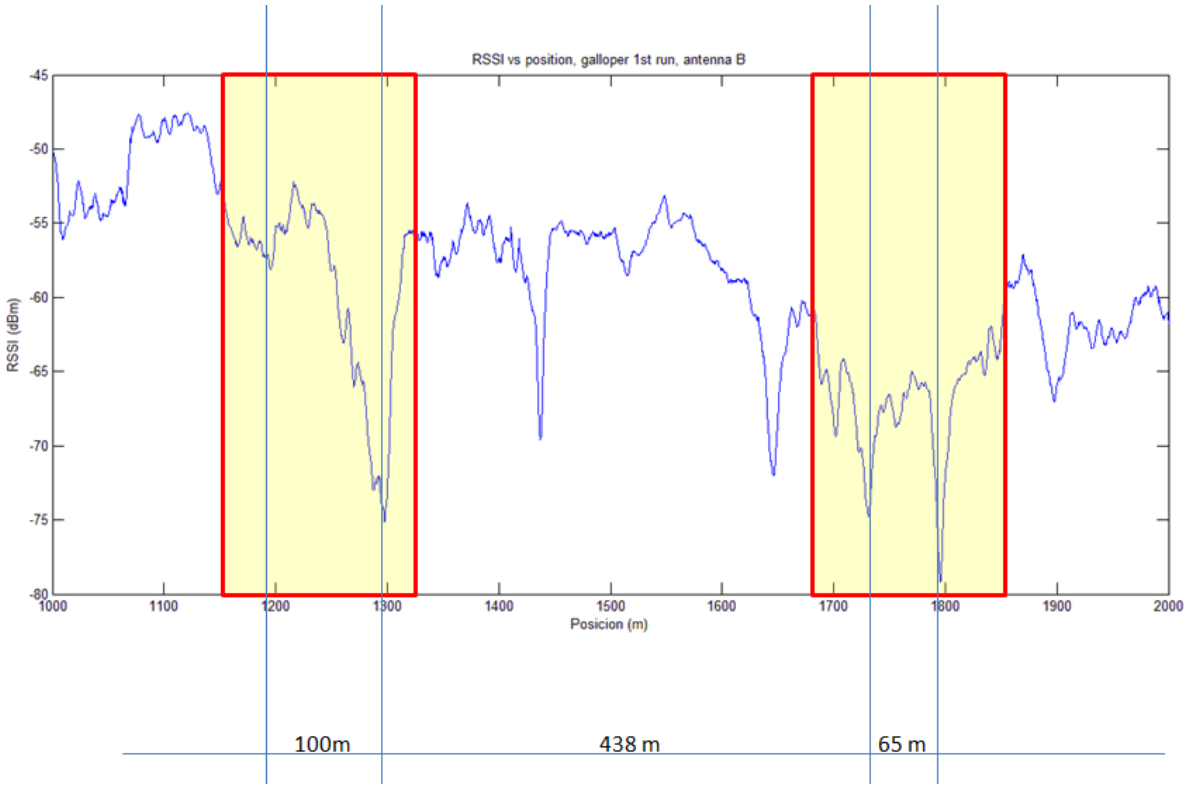

Figure A2. Repeatable fadings for Antenna B in Journey 1.

Antenna C:

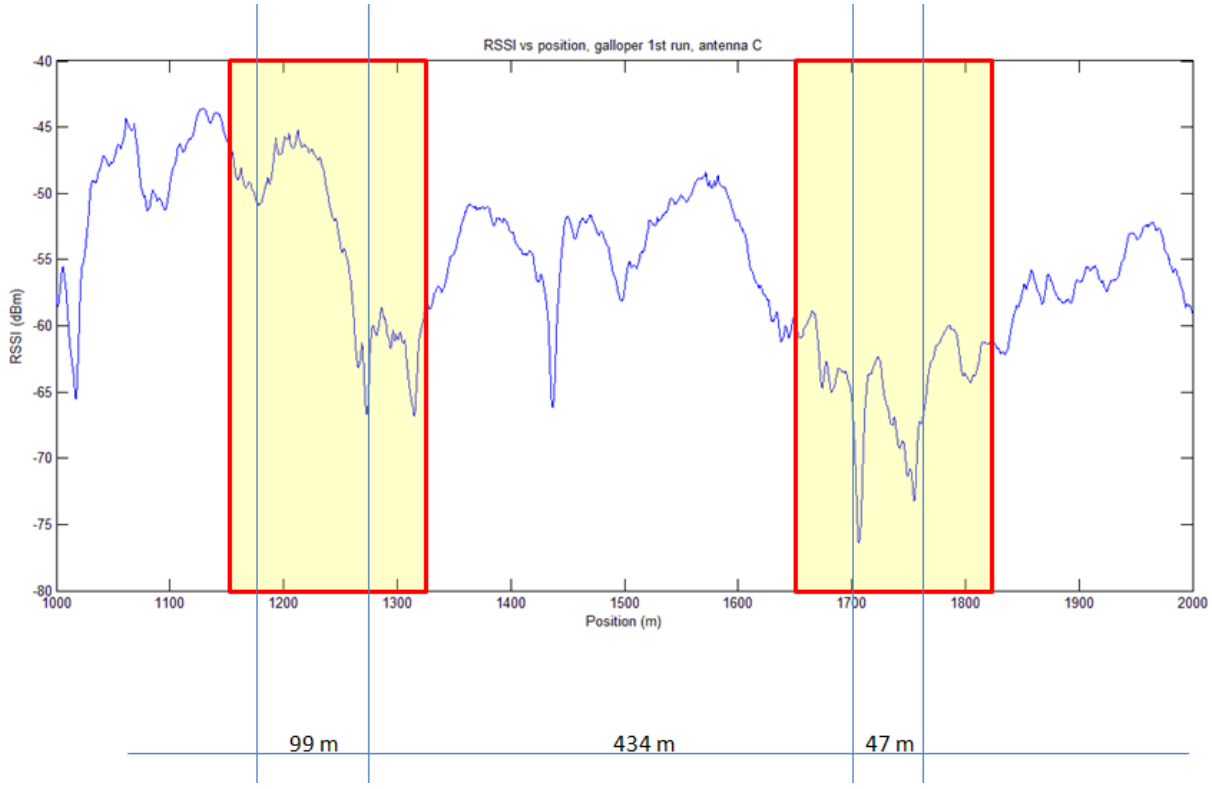

Figure A3. Repeatable fadings for Antenna C in Journey 1.

JOURNEY 3

Antenna A:

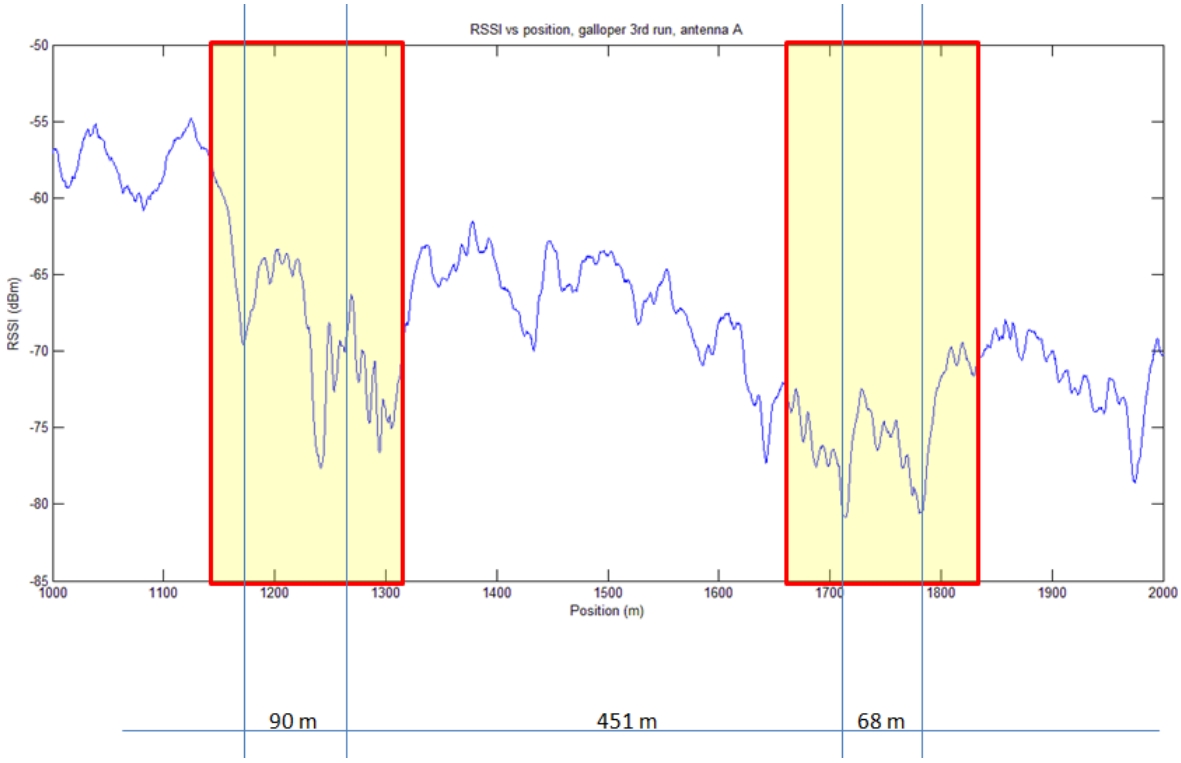

Figure A4. Repeatable fadings for Antenna A in Journey 3.

Antenna B:

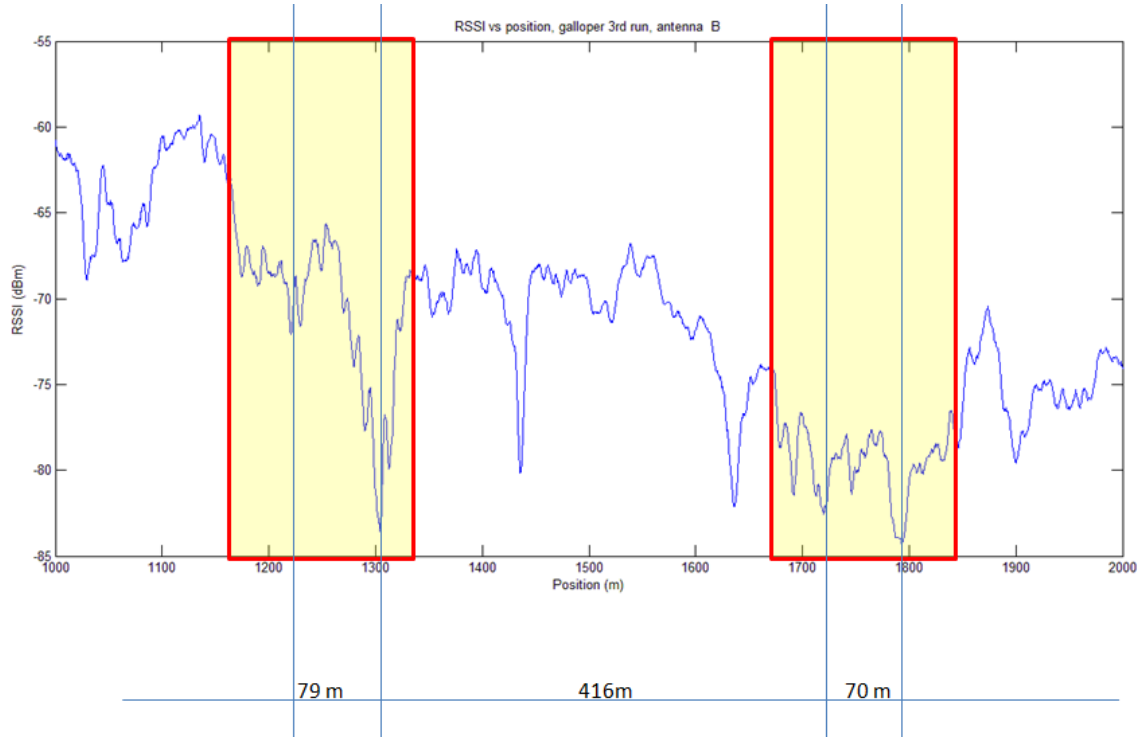

Figure A5. Repeatable fadings for Antenna B in Journey 3.

Antenna C:

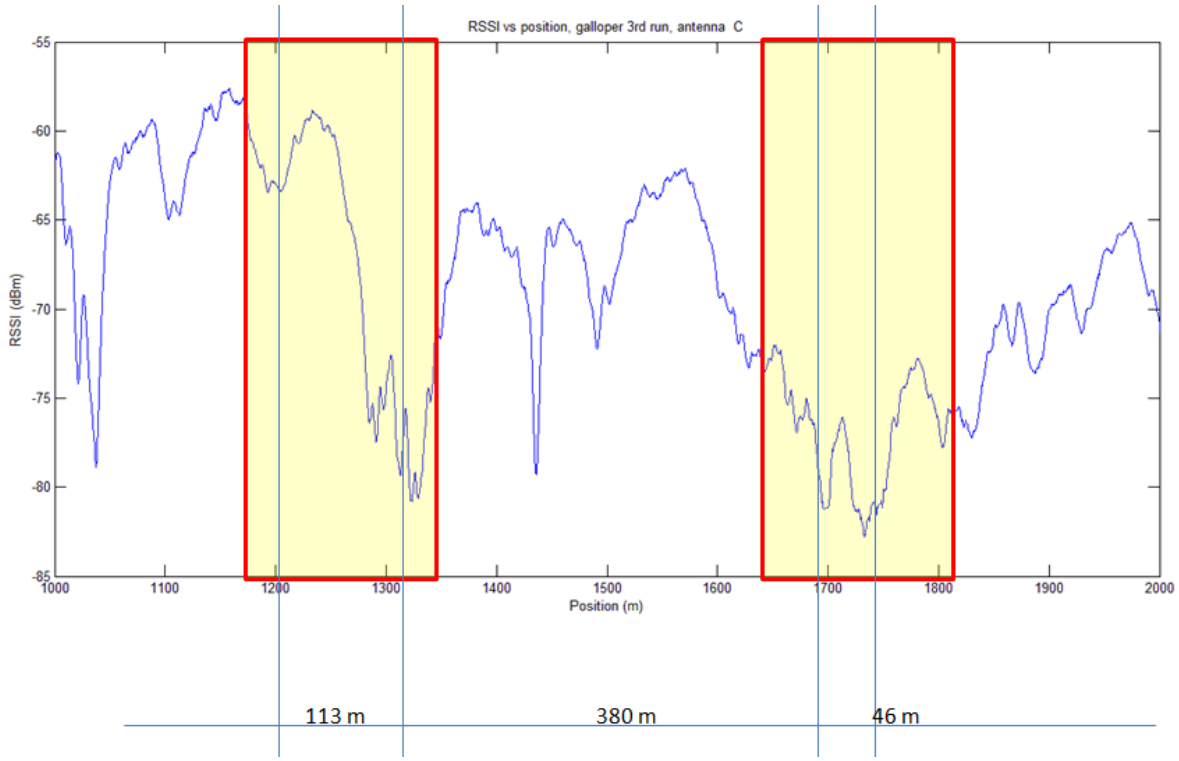

Figure A6. Repeatable fadings for Antenna C in Journey 3.

JOURNEY 4

Antenna A:

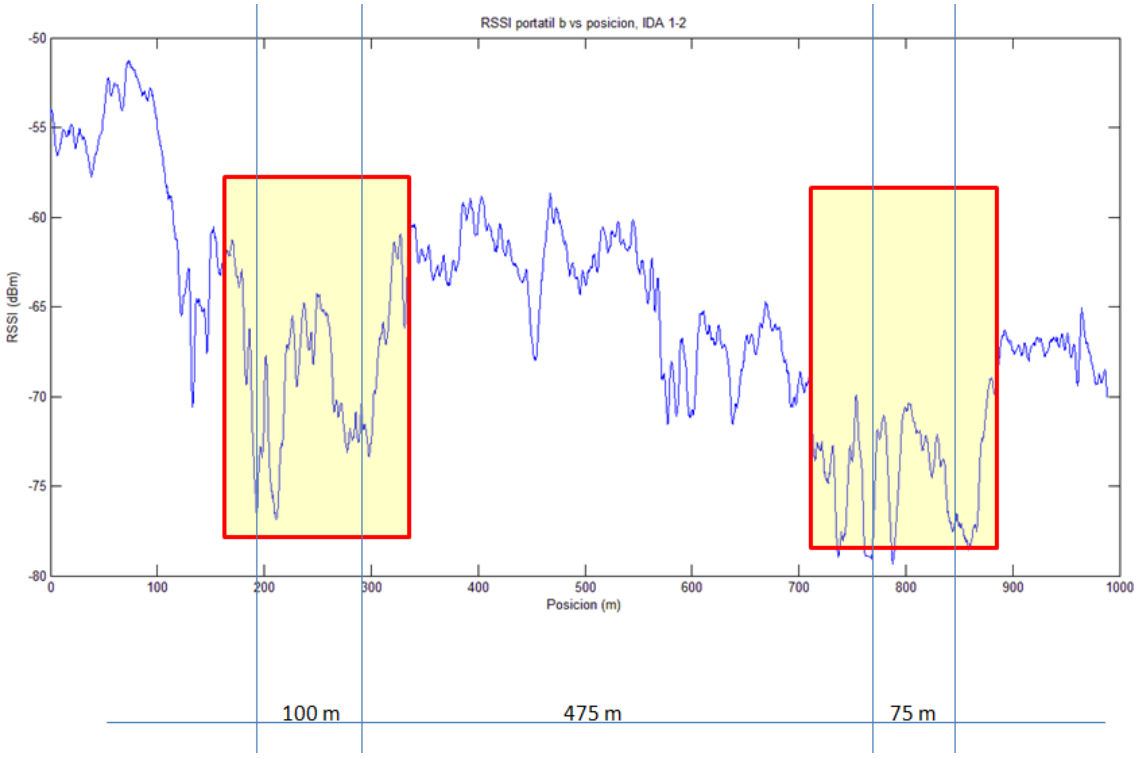

Figure A7. Repeatable fadings for Antenna A in Journey 4.

Antenna B:

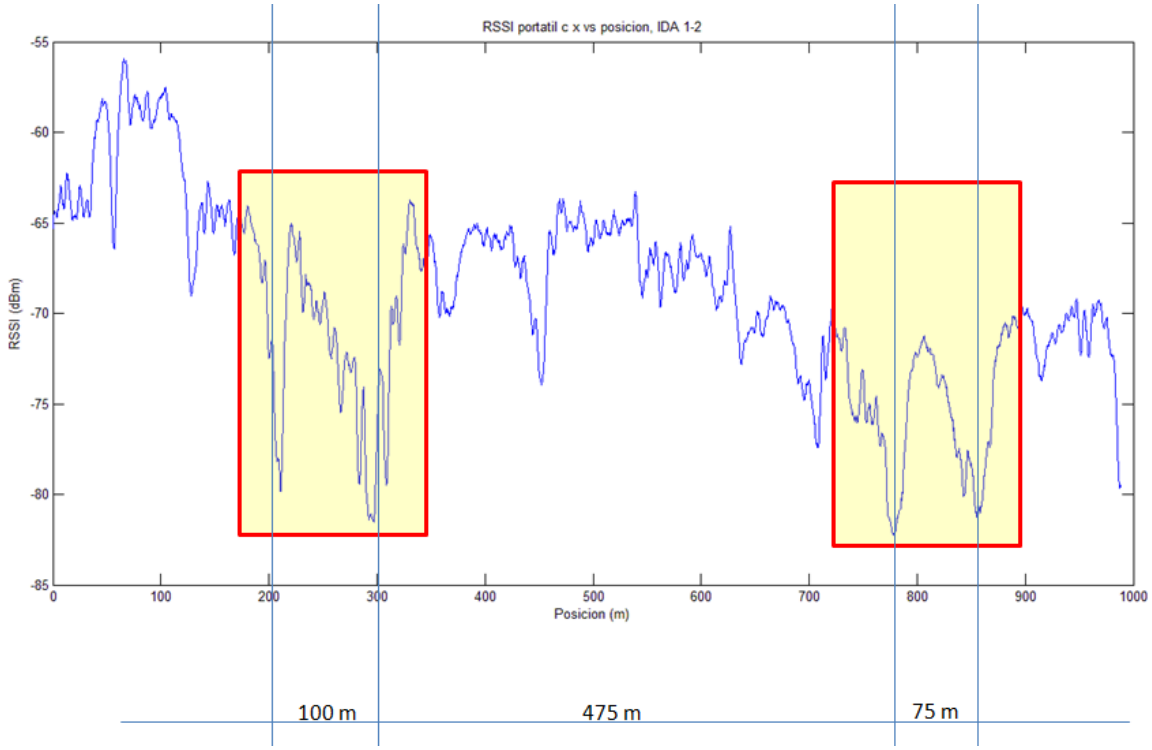

Figure A8. Repeatable fadings for Antenna B in Journey 4.

Antenna C:

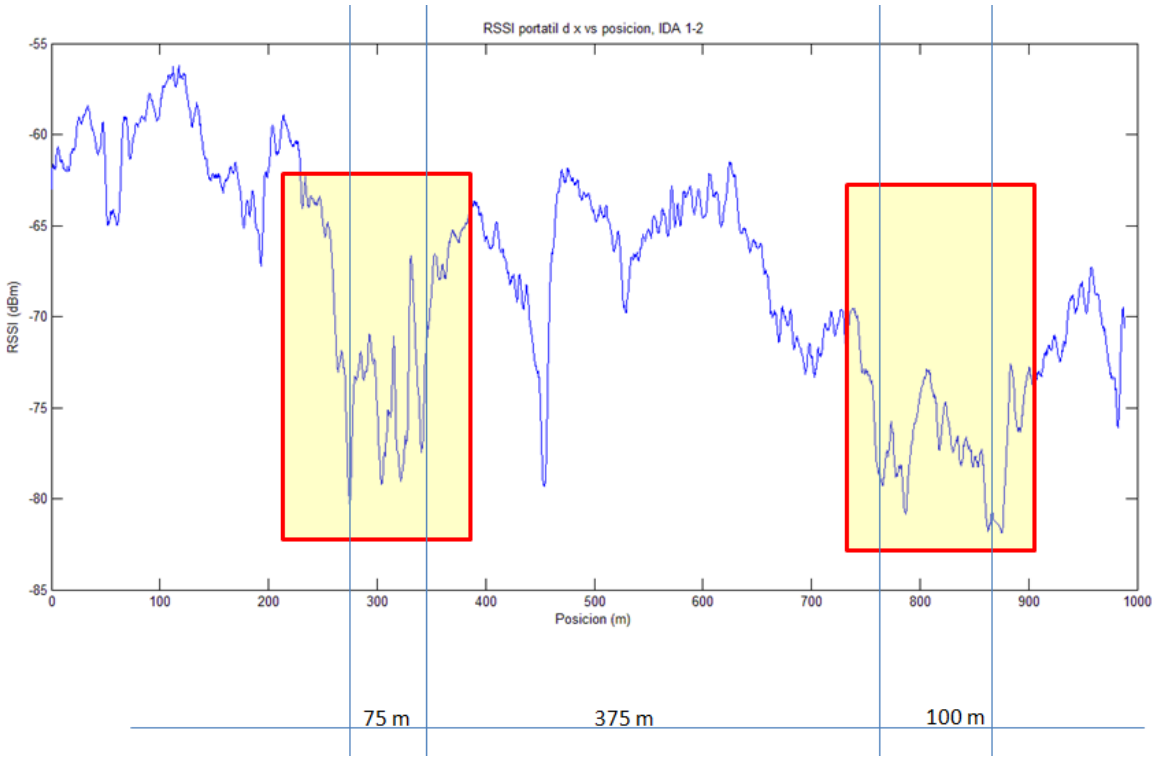

Figure A9. Repeatable fadings for Antenna A in Journey 4.

And a summary where we depict location and distance between fadings, in meters, is depicted in table A.1.

	1st fading	2nd fading	Separation 1st – 2nd	3rd fading	4th fading	Separation 3rd - 4th	Separation 2nd - 3rd
Journey 1	1221	1283	62	1725	1790	65	442
Journey 1	1194	1294	100	1732	1797	65	438
Journey 1	1176	1275	99	1709	1756	47	434
Journey 3	1175	1265	90	1716	1784	68	451
Journey 3	1222	1301	79	1717	1787	70	416
Journey 3	1201	1314	113	1694	1740	46	380
Journey 4	1209	1289	80	1769	1857	88	480
Journey 4	1212	1297	85	1781	1860	79	484
Journey 4	1191	1273	82	1784	1869	85	511

Table A1. Repeatable Fadings Location in Every Journey. All units are in meters.

Appendix B: Influence of Vaults over Propagation

In this case, we highlighted the places were vaults take place, in order to find a pattern of fadings or gain points, if any. Six graphs are presented: one for each of the three antennas, during the first half and second half of the 4th Journey.

As a reminder, SLAM module was implemented in the Small Scale tool, which was used in the "Fadings Zone" and not in the entire "Zone of Interest". For this reason, vaults influence over propagation is analyzed only in this zone (1 Km in length).

For the first half of the Fadings Zone, graphs obtained are depicted in figures

Antenna A:

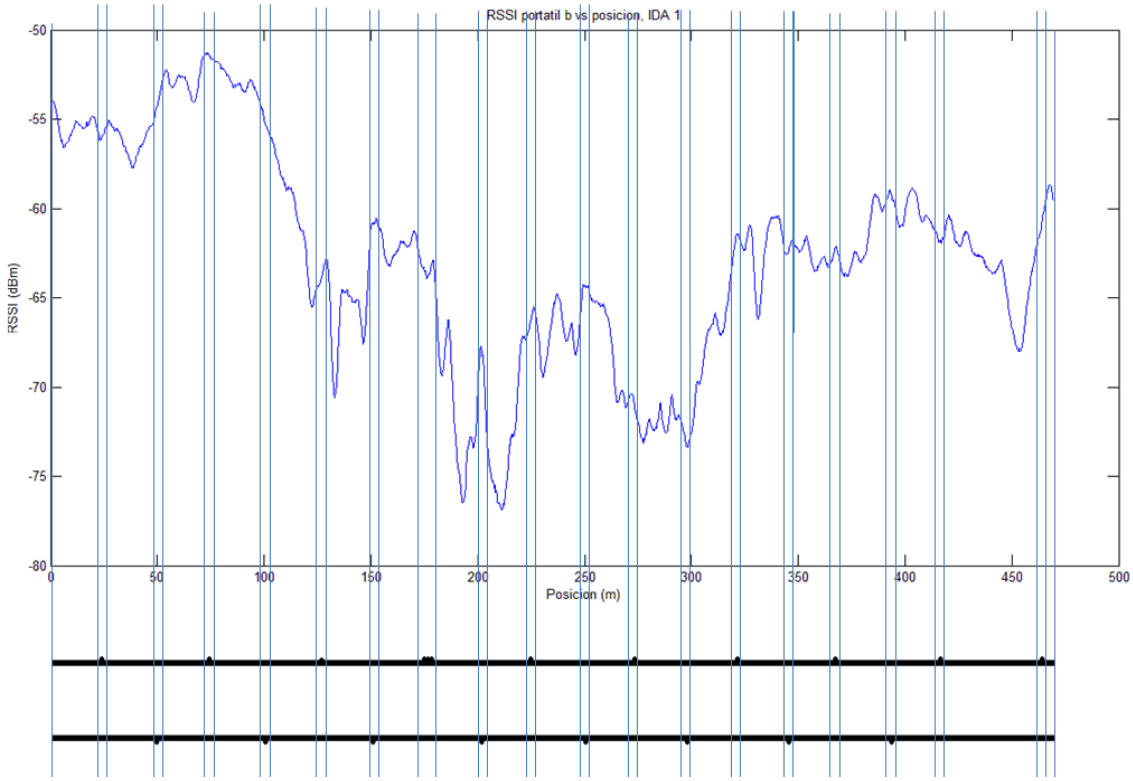

Figure B1. Vaults location for Antenna A in the first half of Journey 4.

Antenna B:

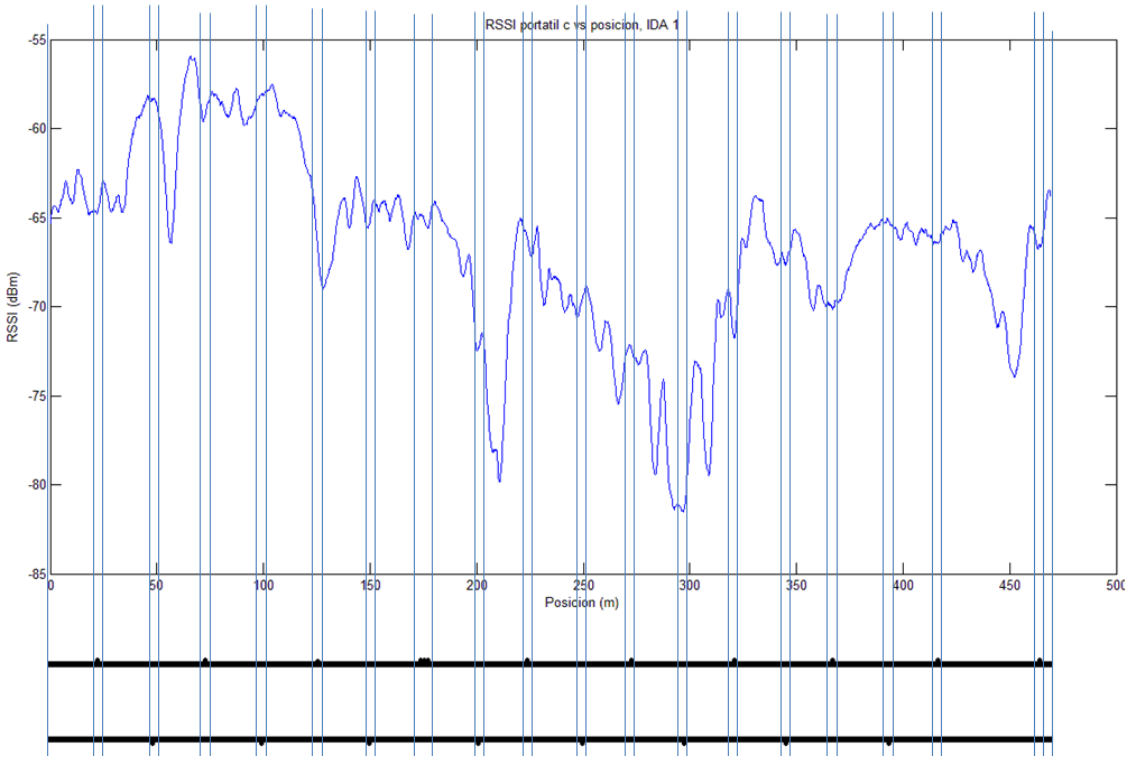

Figure B2. Vaults location for Antenna B in the first half of Journey 4.

Antenna C:

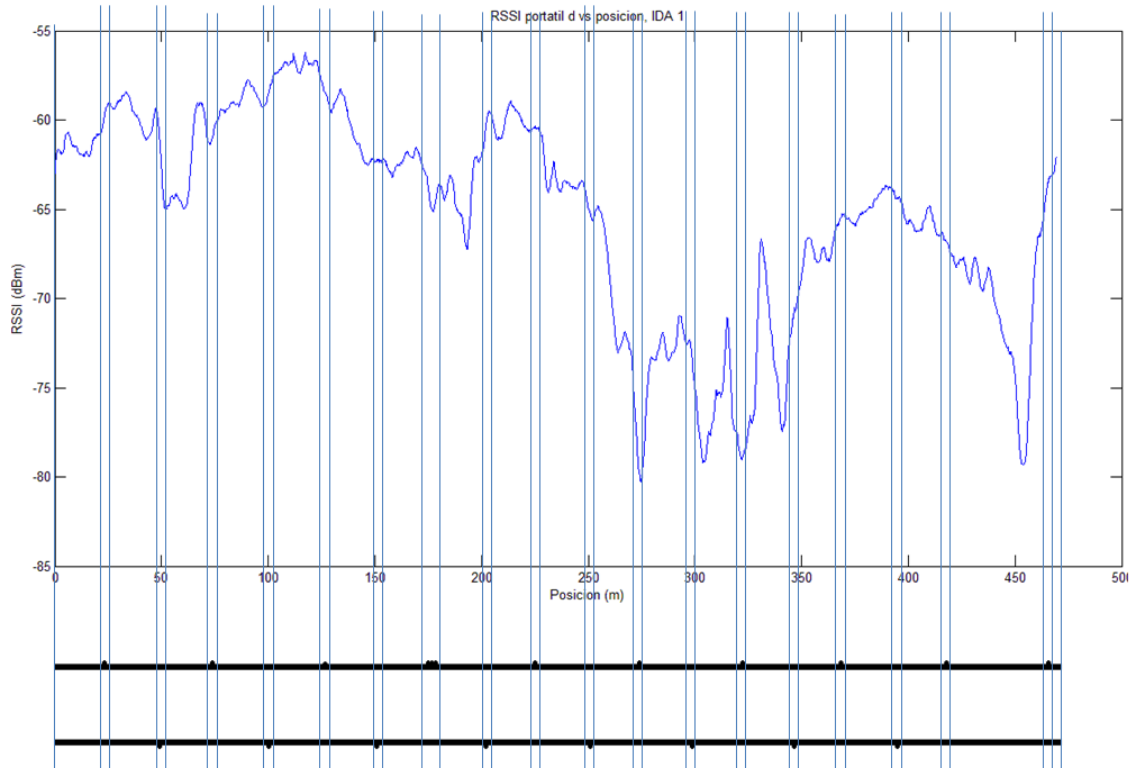

Figure B3. Vaults location for Antenna C in the first half of Journey 4.

For the second half of the Fadings Zone, graphs obtained are depicted in figures

Antenna A:

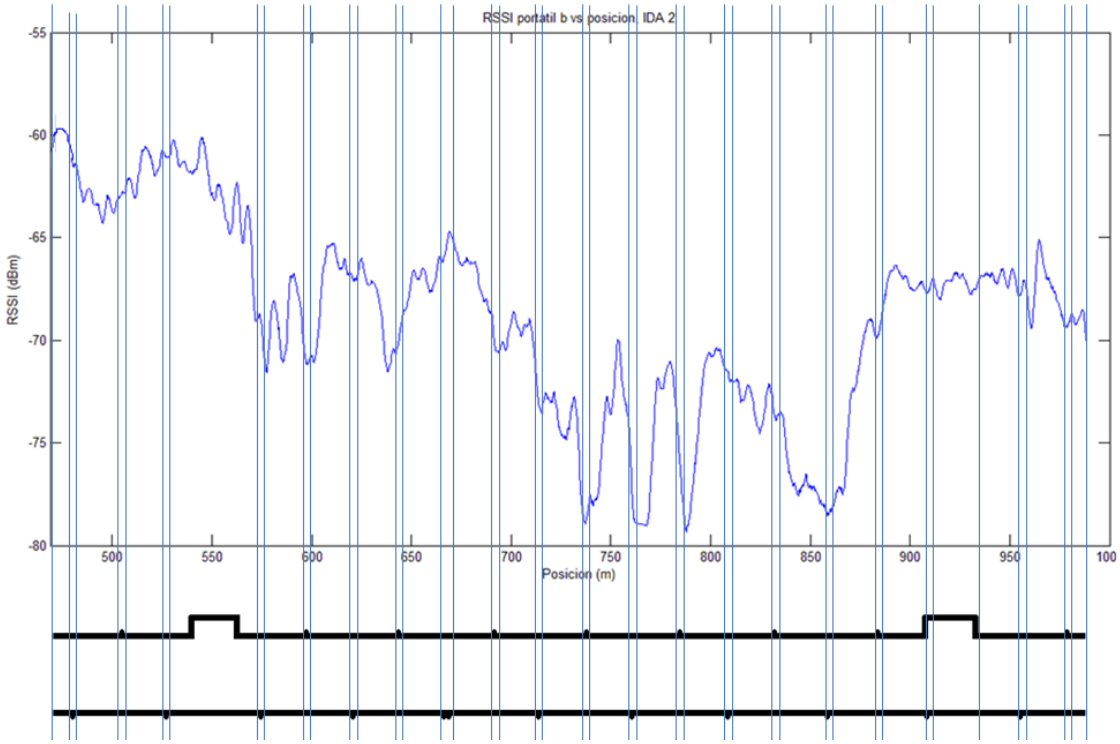

Figure B4. Vaults location for Antenna A in the second half of Journey 4.

Antenna B:

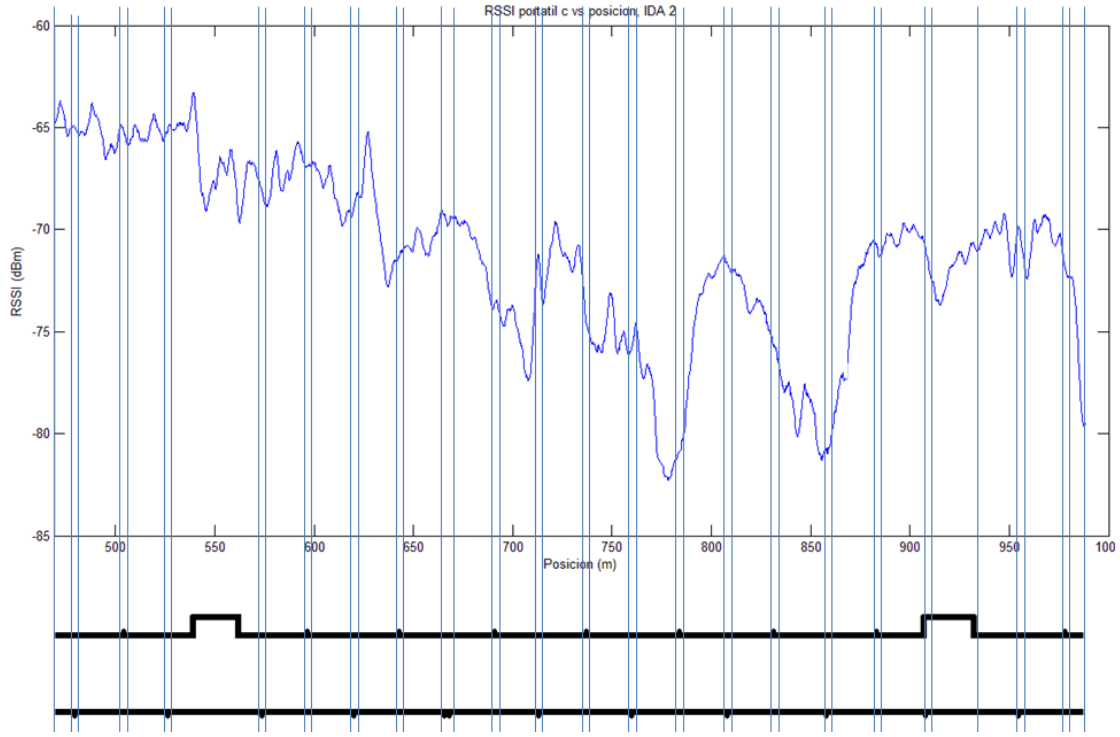

Figure B5. Vaults location for Antenna B in the second half of Journey 4.

Antenna C:

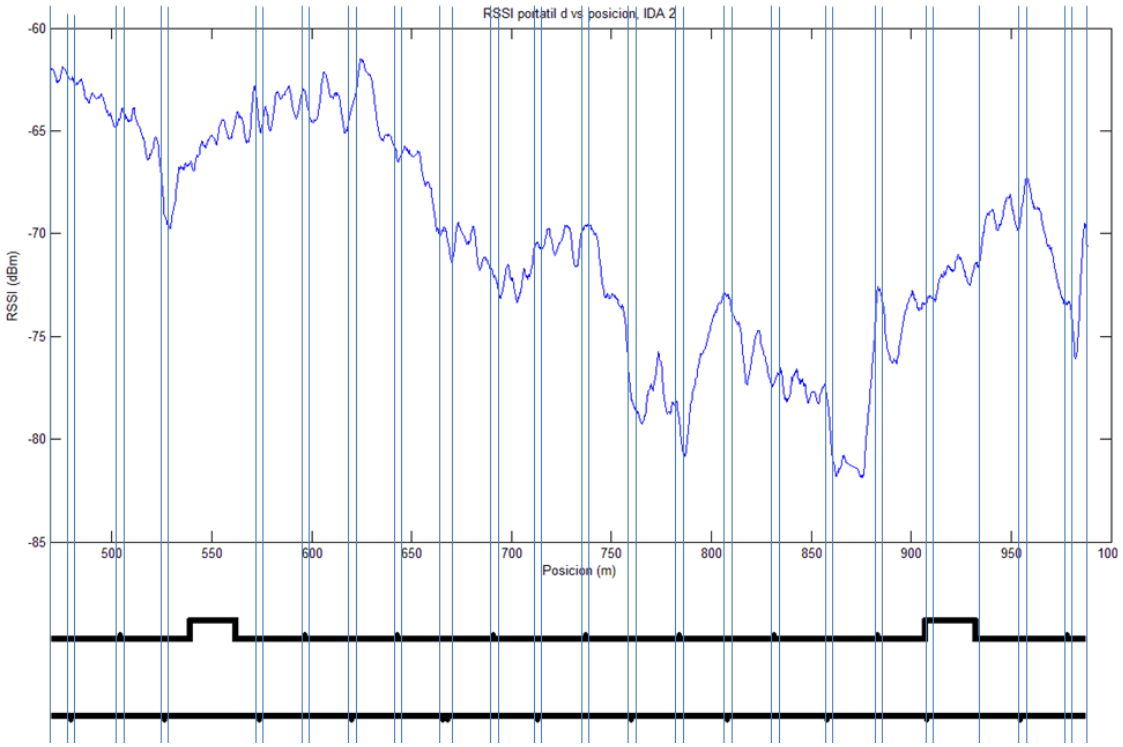

Figure B6. Vaults location for Antenna C in the second half of Journey 4.

It couldn't be found a pattern of influence from vaults over propagation. Casually, some fadings appear where a vault is located, but in the other cases signal remains equal or has a gain. So no specific phenomena are attributed to vaults. Regarding the magnitude of these fadings and gain points, they are from less than 1 dB up to almost 10 dB. Again, these differences are attributed to multipath propagation, instead of vault influence.

Appendix C: Influence of galleries over propagation

We have highlighted the places were galleries take place, in order to find a pattern of fadings or gain points, if any. Three graphs are presented: one for each of the three antennas, during the second half of the 4th Journey. The reason of analyzing these effects only in the second half of the Fadings Zone is because no gallery appeared in the first half.

As a reminder, SLAM module was implemented in the Small Scale tool, which was used in the "Fadings Zone" and not in the entire "Zone of Interest". For this reason, galleries influence over propagation is analyzed only in this zone (1 Km in length).

For the second half of the Fadings Zone, graphs obtained are depicted in figures

Antenna A:

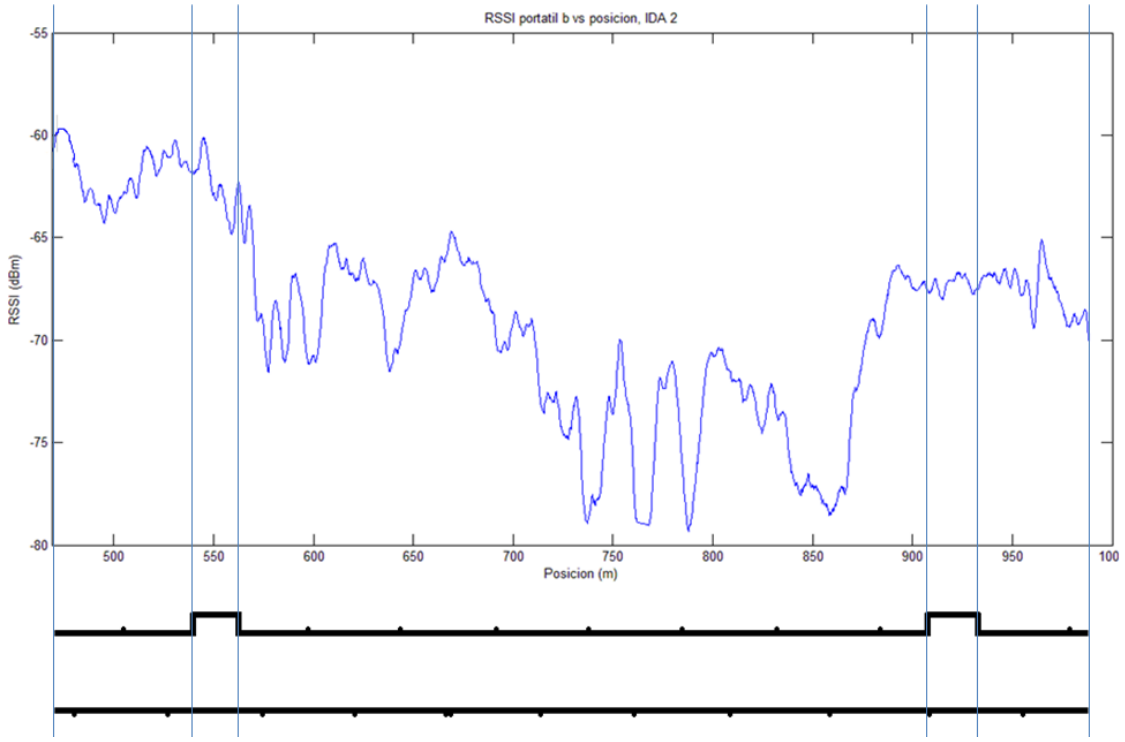

Figure C1. Galleries location for Antenna A in the second half of Journey 4.

Antenna B:

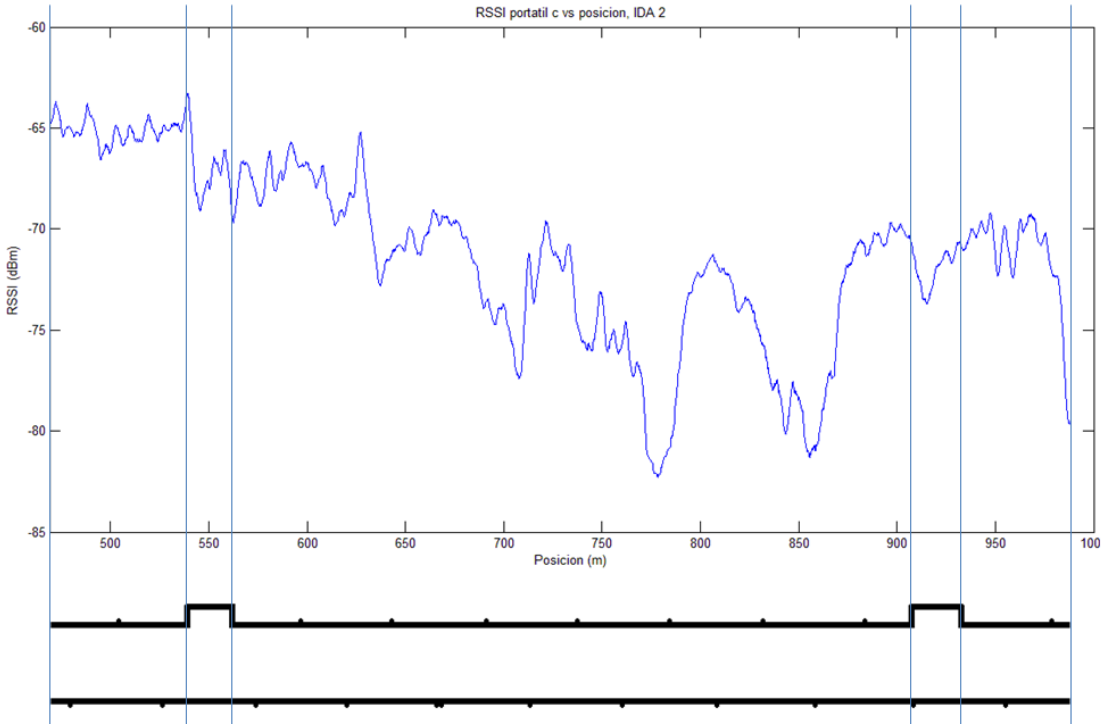

Figure C2. Galleries location for Antenna B in the second half of Journey 4.

Antenna C

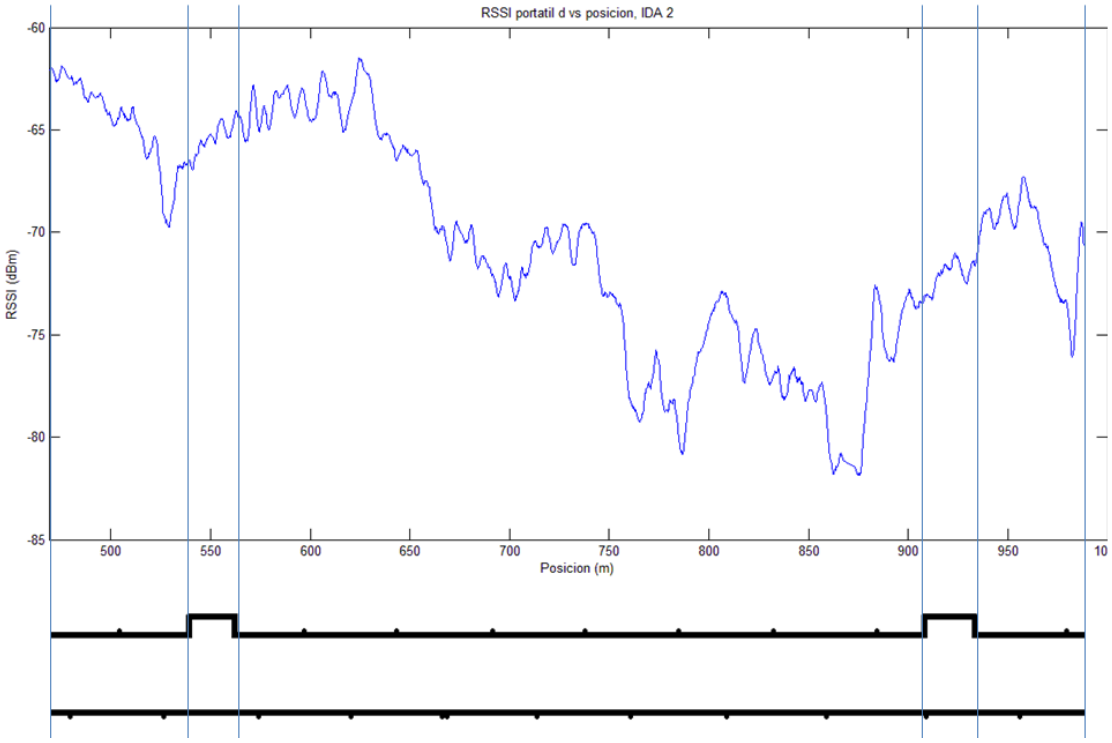

Figure C3. Galleries location for Antenna C in the second half of Journey 4.

It couldn’t be found a pattern of influence from galleries over propagation. Casually, some fadings appear where a gallerie is located (for instance, in Antenna B), but in the other cases signal remains approximately equal (Antenna A) or has a gain (Antenna C). Thus, specific phenomena are attributed to galleries. Again, these differences are attributed to multipath propagation, instead of galleries influence.

Appendix D: Coverage Maps for the Fadings Zone

With the aim of constructing coverage maps, RSSI is discretized in intervals. In this work, we considered convenient to discretize RSSI in 5 dBm intervals, and the start and end values were the minimum and maximum obtained in the RSSI vs Position plots. After this, we assigned a color to each interval, in order to get a visual appreciation of the hazardous zones in terms of position. The obtained the scale is depicted in figure D1.

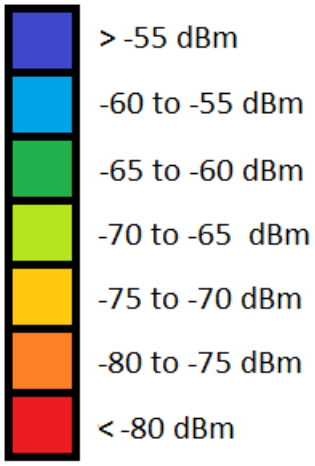

Figure D1. RSSI scale for coverage maps.

Firstly, we build a coverage map for each of the three antennas in each half of the Fadings Zone. Then, a coverage map taking into account spatial diversity was built; this is, taking the best value among the three signals.

For the first half of the Fadings Zones, maps are depicted in figure D2.

Antenna A:

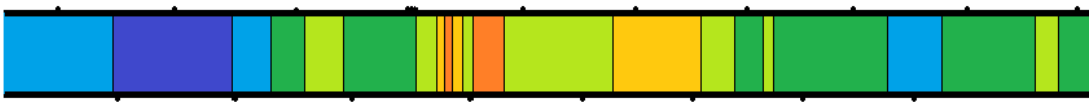

(a)

Antenna B:

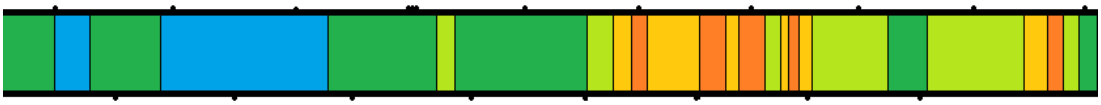

(b)

Antenna C:

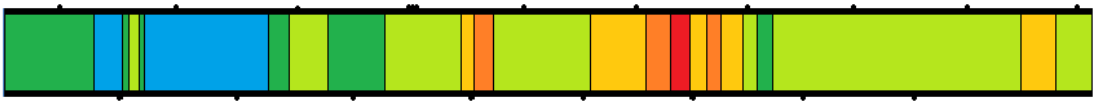

(c)

With diversity:

(d)

Figure D2. Coverage map for antenna A (a), antenna B (b), antenna C (c), and with spatial diversity (d); first half of Fadings Zone.

And for the second half of the Fadings Zones, maps are depicted in figure D3.

Antenna A:

(a)

Antenna B:

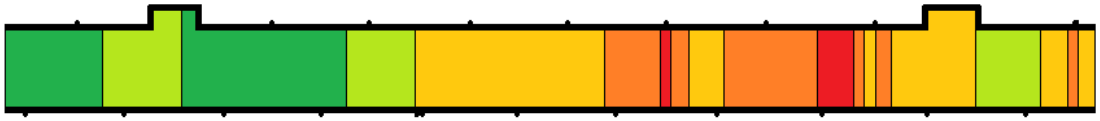

(b)

Antenna C:

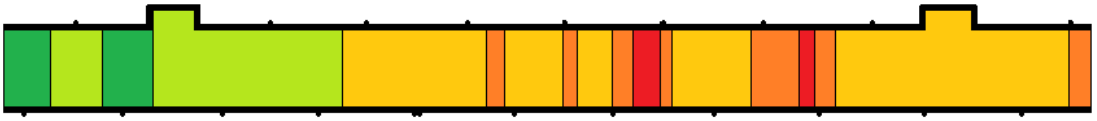

(c)

With diversity:

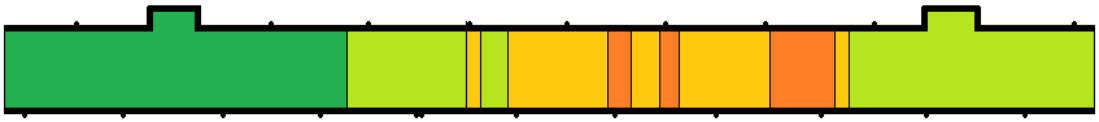

(d)

Figure D3. Coverage map for antenna A (a), antenna B (b), antenna C (c), and with spatial diversity (d); second half of Fadings Zone.

Finally, we represented the whole maps of the Fadings Zone for each antenna, and the spatial diversity map. They are depicted in figure D4.

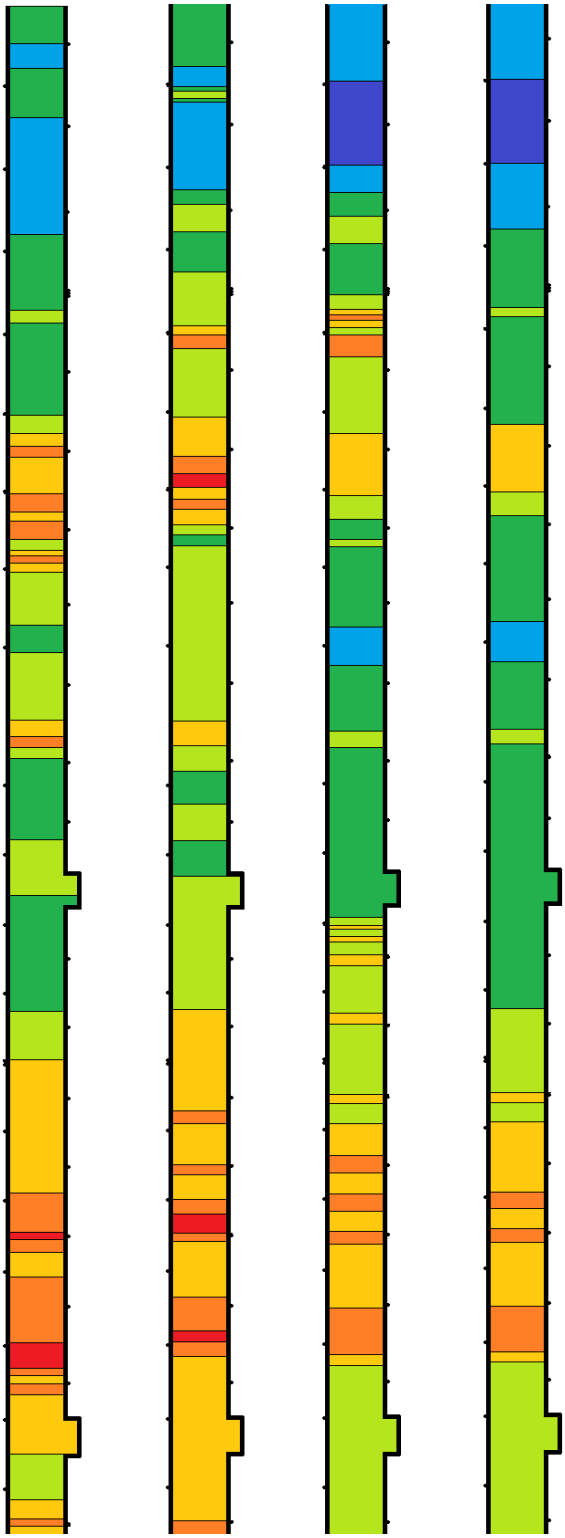

Figure D.4. Complete coverage map for antenna A (a), antenna B (b), antenna C (c), and with spatial diversity (d).

It's clearly evident the importance of spatial diversity. Taking it into account, there aren't hazardous zones (represented in red in the maps), and dangerous zones can be converted into safer regions.

Appendix E: Physical Maps for the Fadings Zone

Maps obtained after running the SLAM algorithm for the first and second half of this zone are presented in figure E.1.

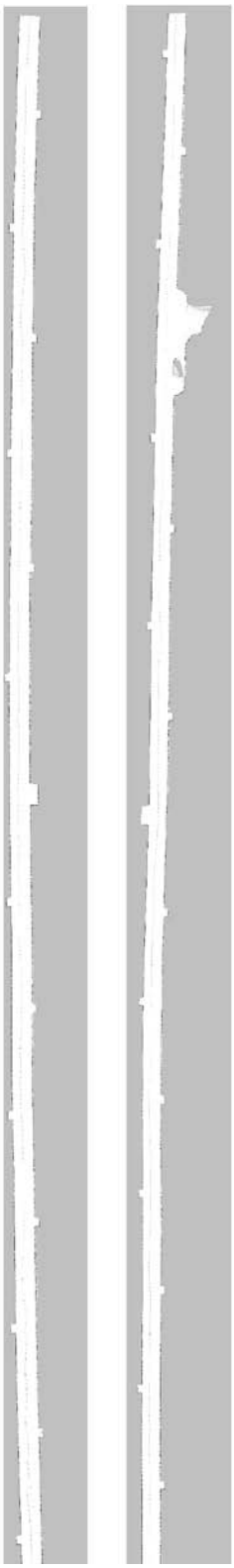

Figure E.1. Physical maps for the first and second half of the Fadings Zone.

And zooming the maps, both vaults and galleries can be appreciated clearly, depicted in figure E.2 and E.3 respectively.

Figure E.2. Vaults in the Physical Map.

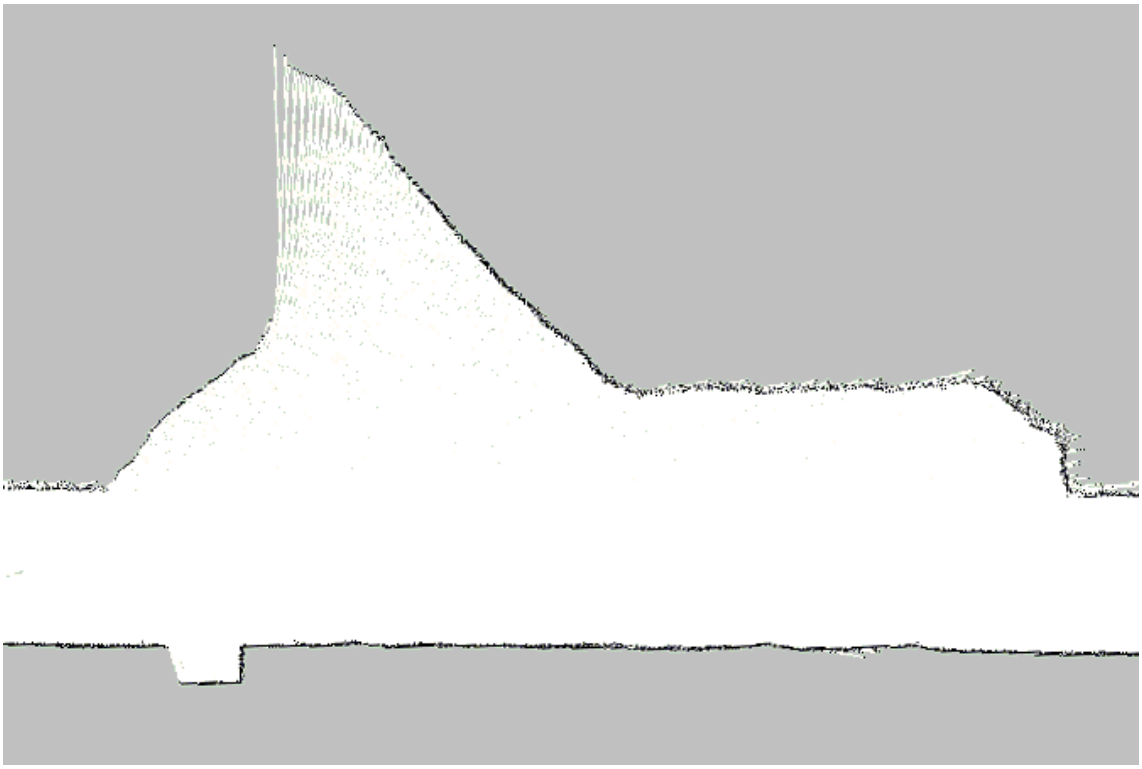

Figure E.3. Gallery in the Physical Map.